

Lawrence Berkeley National Laboratory

LBL Publications

Title

Thermal effects on geologic carbon storage

Permalink

<https://escholarship.org/uc/item/6fg5t8xg>

Authors

Vilarrasa, Victor
Rutqvist, Jonny

Publication Date

2017-02-01

DOI

10.1016/j.earscirev.2016.12.011

Peer reviewed

1 **Thermal effects on geologic carbon storage**

2 **Victor Vilarrasa^{1,2*} and Jonny Rutqvist³**

3 ¹ Institute of Environmental Assessment and Water Research (IDAEA), Spanish National
4 Research Council (CSIC), Jordi Girona 18-26, 08034 Barcelona, Spain

5 ² Associated Unit: Hydrogeology Group (UPC-CSIC)

6 ³ Lawrence Berkeley National Laboratory (LBNL), 1 Cyclotron Rd, Berkeley, CA 94720,
7 USA

8
9
10 **Accepted for publication in Earth-Sciences Reviews**

11 **December 15, 2016**

12 <https://doi.org/10.1016/j.earscirev.2016.12.011>
13

14
15
16
17
18
19
20
21
22
23 * Corresponding author: victor.vilarrasa@upc.edu

24 **ABSTRACT**

25 One of the most promising ways to significantly reduce greenhouse gases emissions, while
26 carbon-free energy sources are developed, is Carbon Capture and Storage (CCS). Non-
27 isothermal effects play a major role in all stages of CCS. In this paper, we review the literature
28 on thermal effects related to CCS, which is receiving an increasing interest as a result of the
29 awareness that the comprehension of non-isothermal processes is crucial for a successful
30 deployment of CCS projects. We start by reviewing CO₂ transport, which connects the regions
31 where CO₂ is captured with suitable geostorage sites. The optimal conditions for CO₂
32 transport, both onshore (through pipelines) and offshore (through pipelines or ships), are such
33 that CO₂ stays in liquid state. To minimize costs, CO₂ should ideally be injected at the
34 wellhead in similar pressure and temperature conditions as it is delivered by transport. To
35 optimize the injection conditions, coupled wellbore and reservoir simulators that solve the
36 strongly non-linear problem of CO₂ pressure, temperature and density within the wellbore and
37 non-isothermal two-phase flow within the storage formation have been developed. CO₂ in its
38 way down the injection well heats up due to compression and friction at a lower rate than the
39 geothermal gradient, and thus, reaches the storage formation at a lower temperature than that
40 of the rock. Inside the storage formation, CO₂ injection induces temperature changes due to
41 the advection of the cool injected CO₂, the Joule-Thomson cooling effect, endothermic water
42 vaporization and exothermic CO₂ dissolution. These thermal effects lead to thermo-hydro-
43 mechanical-chemical coupled processes with non-trivial interpretations. These coupled
44 processes also play a relevant role in “Utilization” options that may provide an added value to
45 the injected CO₂, such as Enhanced Oil Recovery (EOR), Enhanced Coal Bed Methane
46 (ECBM) and geothermal energy extraction combined with CO₂ storage. If the injected CO₂
47 leaks through faults, the caprock or wellbores, strong cooling will occur due to the expansion

48 of CO₂ as pressure decreases with depth. Finally, we conclude by identifying research gaps
49 and challenges of thermal effects related to CCS.

50

51 Keywords: CO₂ transport; injection schemes; CO₂ storage; thermo-hydro-mechanical-
52 chemical couplings; induced microseismicity; caprock integrity; well integrity; CO₂ leakage

53

54

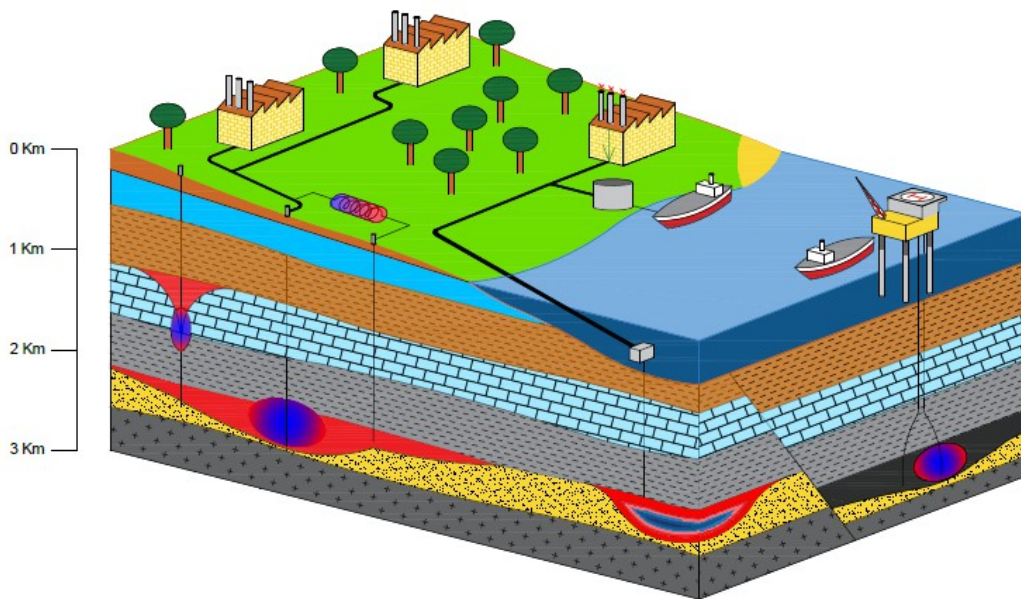
55 **1. INTRODUCTION**

56 Huge amounts of greenhouse gases, especially carbon dioxide (CO₂), are emitted to the
57 atmosphere each year (around 36 Gt were emitted in 2014) as a result of burning fossil fuels
58 for energy production (Le Quéré et al., 2016). These greenhouse gases retain the heat coming
59 from the sun, which alters atmospheric circulations and therefore, the climate. To mitigate the
60 negative effects of anthropogenic climate change, we should act quickly to significantly
61 reduce these emissions. One of the most promising ways to reduce greenhouse gases
62 emissions, at least in the short-term, while carbon-free energy sources are developed, is
63 Carbon Capture and Storage (CCS) (IPCC, 2005). CCS consists in capturing CO₂ from the
64 main point sources (e.g., steel and cement industries and coal and gas-fired power plants),
65 transport the captured CO₂ to the injection wells and store it in deep geological formations.

66 CCS implies compression and expansion processes that cause pressure and temperature of
67 CO₂ to vary over a wide range of values. During these variations, CO₂ may be present in
68 gaseous, liquid or supercritical state. CO₂ properties, i.e., density, viscosity, specific heat
69 capacity and enthalpy (Span and Wagner, 1996; Pruess and Garcia, 2002), as well as its
70 solubility on water and brine (Duan and Sun, 2003; Harvey, 1996; Koschel et al., 2006) are
71 strongly dependent on pressure and temperature. To reproduce these properties, the cubic
72 equation of state of Redlich and Kwong (1949), with parameters adapted for CO₂ (Spycher et

73 al., 2003, 2005), is usually used for its simplicity and because good predictions are obtained
74 (McPherson et al., 2008). Nevertheless, the equation of state of Span and Wagner (1996) is
75 the most accurate one, but at the expenses of a high computational cost derived from the high
76 complexity of its algorithm (Böttcher et al., 2012). Regardless of the equation of state that is
77 considered, the strong dependency of CO₂ properties on pressure and temperature complicates
78 the processes that occur in CCS.

79 Non-isothermal effects play a major role in all stages of CCS (Figure 1). However, to
80 facilitate the understanding and solution of CCS processes, isothermal conditions have been
81 usually considered. As a result, most of the knowledge gained on the processes involved in
82 CCS neglects thermal effects. Nevertheless, the awareness that the comprehension of non-
83 isothermal processes is crucial for a successful deployment of CCS projects has recently
84 motivated an increasing interest to understand thermal effects.



85

86 Figure 1. Schematic representation of thermal effects on CCS.

87 In this review, we present the state-of-the-art of the thermal effects related to CO₂
88 transport, injection, storage and leakage. First, we detail CO₂ transport both onshore and
89 offshore. Next, we present CO₂ injection options and how CO₂ properties change inside the

90 injection well. Then, we focus on CO₂ storage in deep geological formations, looking at
91 thermo-mechanical and thermo-chemical coupled processes and to options of utilization that
92 provide an added value to the injected CO₂. Furthermore, we elaborate on potential CO₂
93 leakage through wells and faults. Finally, we conclude by identifying the existing research
94 gaps and challenges related to thermal effects on geologic carbon storage.

95

96 **2. CO₂ TRANSPORT**

97 While CO₂ is mainly emitted onshore, both onshore and offshore geological formations
98 may be suitable for storage. In general, CO₂ will have to be transported from the sources
99 where it will be captured up to the storage sites. The optimum CO₂ transport options differ for
100 onshore and offshore transportation. While for onshore transportation pipelines are the only
101 feasible option (Svensson et al., 2004), both pipelines and ships can provide good solutions
102 for offshore transportation. Though other options exist for onshore transportation, such as
103 motor carriers and railways, they are not competitive because they are very expensive and of
104 limited capacity (Skovholt, 1993). As for offshore transportation, ships are more flexible than
105 pipelines, but require intermediate storage facilities, such as steel tanks or underground
106 caverns, at harbors. On the other hand, pipelines require fewer logistics than ships and provide
107 a continuous flow rate, but they imply building a new infrastructure on the seabed (Svensson
108 et al., 2004).

109 Optimal marine transport conditions are obtained in semi-pressurized vessels of around
110 20,000 m³ in liquid conditions close to the triple point, at 0.65 MPa and -52 °C (Aspelund et
111 al., 2006). These conditions yield CO₂ densities around 1,100 kg/m³, which optimize the
112 transport in terms of volume. The most expensive process for ship transport is the liquefaction
113 and gas conditioning previous to filling the ships. But costs could be reduced by using the
114 liquid conditions of onshore pipelines when arriving at harbors for loading the ships. The

115 efficiency of the system could be improved further by recovering CO₂ cold energy with a
116 Rankine cycle during ship delivery, in which CO₂ has to be heated up to avoid injectivity
117 issues due to ice or hydrate formation in the storage formation (You et al., 2014).

118 In pipelines, the best way to transport CO₂ is also in liquid state (McCoy and Rubin, 2008).
119 Transport in gas phase is non-economical because of its low density, which requires large
120 diameter pipes and implies high pressure drops. Pressure drop depends on the flow rate and
121 the geometric characteristics of the pipe, i.e., diameter, length, elevation gain. Transport of
122 supercritical CO₂ is preferable to transport of gaseous CO₂, but still, it induces a higher
123 pressure drop than in liquid conditions, causing a decrease in density and thus, an increase in
124 velocity, which, in turn, enhances the pressure drop. This enhanced pressure drop would lead
125 to shorter distances between booster stations. Booster stations should be placed such that two-
126 phase flow is avoided within the pipeline. Actually, operation of pipelines onshore may
127 present difficulties in hilly terrain because pressure will decrease at the top of the hills, where
128 CO₂ may turn into gas, giving rise to a two-phase flow, which is complicated to handle
129 (Skovholt, 1993). Thus, transport of CO₂ is preferable in liquid state rather than in
130 supercritical conditions due to the lower compressibility and higher density of liquid CO₂.
131 Though liquid CO₂ has a higher viscosity than supercritical CO₂ (around 30%), CO₂ transport
132 in liquid conditions permits using smaller pipe diameters, leading to lower pressure drops and
133 thus, a more efficient transport (McCoy and Rubin, 2008; Nimitz et al., 2010).

134 To maintain liquid conditions, burying CO₂ pipelines can help controlling operation
135 pressure and temperature conditions because underground temperature is more stable than
136 surface temperature. In warm climates, where ground surface temperature can reach 65 °C at
137 noon, the temperature 1 m underground remains below 30 °C (Zhang et al., 2006). Despite the
138 higher installation costs derived from burying pipelines, the higher energy efficiency will
139 offset the initial investment because operation costs are around 15 % lower for liquid than for

140 supercritical CO₂ transport (Zhang et al., 2006). Alternatively, in warm climates, insulating the
141 pipeline and cooling the CO₂ to maintain liquid conditions may prove economical because of
142 the lower pressure drop and therefore, lower number of booster stations for repressurizing
143 CO₂ (Zhang et al., 2006). Furthermore, if CO₂ remains in liquid state, pumps, which are easier
144 to operate than compressors, can be used to boost pressure. But apart from operational and
145 economic reasons, pipelines will likely be buried for environmental, security and safety
146 reasons.

147 CO₂ is not toxic, but it can be fatal if its concentration exceeds 10 % by volume because
148 CO₂ produces asphyxia (Baxter et al., 1999). CO₂ could accumulate in depressions if there
149 were a CO₂ leakage in a pipeline because CO₂ is heavier than air. Since CO₂ is colorless and
150 odorless, humans and animals cannot detect CO₂ leakage and accumulation. Adding
151 mercaptans, which people can easily identify because they are already added to natural gas,
152 would be very beneficial because people could quickly react in case of CO₂ leakage (Gale and
153 Davison, 2004). Nevertheless, an advisable practice would be to construct pipelines avoiding
154 human settlements and to place CO₂ detectors along pipelines.

155 Other safety issues are related to the depressurization of a pipeline, either because it fails or
156 due to planned maintenance. In such case, CO₂ will experience a phase change (from liquid to
157 gas) which will cause a strong cooling. Such cooling should be taken into account in pipeline
158 design to avoid brittle failure. This cooling may be limited by adding impurities to CO₂. For
159 example, Munkejord et al. (2010) found that, for CO₂ mixtures with CH₄, the cooling due to
160 evaporation becomes lower as the CO₂ content decreases. However, impurities may lead to
161 enhanced pipe corrosion.

162 The construction of pipelines for CO₂ transport should be planned carefully because scale
163 effects are relevant. For example, large diameter pipelines are much cheaper to operate than
164 several small pipelines with equivalent capacity. Thus, it is advisable to do a strategic

165 planning to connect the source points where CO₂ will be captured with the storage regions
166 using a single large pipeline, rather than several smaller pipelines. A significant experience
167 with CO₂ pipelines exists in the USA, where an extensive CO₂ pipeline infrastructure (several
168 thousands of km) already exists, mainly carrying naturally occurring CO₂ for enhanced oil
169 recovery (EOR). These pipelines have proven to be safe in terms of potential for CO₂ release
170 and thus, they do not represent a serious public hazard (Gale and Davison, 2004).

171

172 3. INJECTION OPTIONS

173 Since CO₂ will remain in supercritical conditions at the pressure and temperature
174 conditions of storage formations, it is usually assumed that CO₂ will be injected in
175 supercritical state. However, CO₂ needs to be transported from the source points, which are
176 usually large industries or power plants, to the injection wells, which will likely be separated
177 by several tens or even hundreds of km. CO₂ transport will be done through pipelines if it is
178 onshore or through ships or pipelines if it is offshore. The optimum conditions for
179 transporting CO₂ is in liquid conditions both for pipelines and ships (see Section 2). Thus,
180 CO₂ will reach the wellhead in liquid state. For this reason, injecting in liquid state seems the
181 most reasonable option.

182 Liquid CO₂ injection has some advantages. Silva et al. (2011), who proposed to inject CO₂
183 directly in liquid state, showed that liquid CO₂ injection is an energetically efficient injection
184 concept. For the pressure and temperature ranges typical of injection wells, the density of
185 liquid CO₂, which may reach values close to those of water density (in the order of 750 to 950
186 kg/m³), is significantly higher than that of supercritical CO₂ (in the order of 250 to 700 kg/m³)
187 (Figure 2). Thus, just by gravity, liquid CO₂ flows downwards more easily, which implies that
188 a lower compression energy is required to inject CO₂ (Vilarrasa et al., 2013). However, liquid
189 CO₂ injection has been feared because of its cold temperature, which induces thermal

190 contraction and associated stress reduction that may cause fracture instability in the storage
191 formation, the caprock, and/or the wellbore.

192 Thermal stresses induced by temperature difference between the wellbore and the
193 surrounding rock may lead to casing failure (Teodoriu, 2015). These stresses may become
194 large if the temperature change in the wellbore is large and fast (Kaldal et al., 2015).
195 Furthermore, if thermal cycling occurs as a result of alternating periods of CO₂ injection
196 (cooling) with shut-downs (heating), radial fractures or debonding of the cement may occur,
197 which could lead to CO₂ leakage (Roy et al., 2016). To minimize the risk of damaging the
198 cement, the use of non-shrinking cements is recommendable (McCulloch et al., 2003).

199 Apart from the cold temperature, the high pressure of liquid CO₂ has also been suspected
200 to potentially induce stability issues in the storage formation and caprock. Nimtz et al. (2010)
201 argued that liquid CO₂ might fracture the storage formation and caprock due to the high
202 overpressure that liquid injection would induce. However, Nimtz et al. (2010) did not couple
203 the pressure at the bottom of the injection well resulting from CO₂ injection along the
204 wellbore with the pressure at the injection well induced by CO₂ injection into the reservoir.
205 Actually, when coupling the wellbore simulator with the reservoir simulator, it has been
206 shown that the injection of 1 Mt/yr of CO₂ in a 100 m-thick reservoir with a permeability of
207 10⁻¹³ m² can be done maintaining liquid conditions along the wellbore and without inducing a
208 large overpressure in the reservoir (Vilarrasa et al., 2013). Thus, excessive overpressure is not
209 necessarily an issue of liquid CO₂ injection. Nevertheless, thermal effects may still be a
210 concern (see Section 5b). But to avoid cooling in the reservoir, and thus, inject in supercritical
211 conditions, CO₂ would need to be heated. At Ketzin, Germany, CO₂ was heated before
212 injecting it, leading to a temperature at the bottom of the injection well slightly higher than
213 that of the reservoir (Liebscher et al., 2013). The CO₂ injection rates at the pilot test site of
214 Ketzin were lower than 1 kg/s, so the energetic cost of heating was not excessive. However, at

215 industrial scale, heating would dramatically increase the energetic cost of injection in CO₂
216 storage projects (Möller et al., 2014; Goodarzi et al., 2015). Goodarzi et al. (2015) estimated
217 the cost of heating to avoid cooling the reservoir in 0.75 \$/m³, which for an injection of 1
218 Mt/yr would represent a heating cost higher than 1 million dollars per year.

219 Pipelines can also be used for transporting CO₂ offshore. In this case, the pipeline lies on
220 the seabed and CO₂ thermally equilibrates with the seawater. Seawater is usually below the
221 CO₂ critical temperature, i.e., 31.04 °C, and thus, liquid conditions will be easily maintained
222 within the pipeline. The transported liquid CO₂ will generally be injected directly into the
223 injection well, as happened at Snøhvit, Norway (Hansen et al., 2013). At Snøhvit, the water of
224 the North Sea is cold (about 4 °C at the seabed), so the compression costs for injecting CO₂
225 are minimized because CO₂ has a high density at these temperatures.

226 When offshore transport is done through ships, CO₂ stays at -52 °C. If CO₂ injection is
227 performed just by compressing CO₂ as it arrives in the ship, CO₂ would reach the storage
228 formation at a temperature well below that of hydrate formation (around 12 °C) and freezing
229 (around 0 °C) temperatures, which would block the pores surrounding the injection well
230 (Krogh et al., 2012). To heat up CO₂ before injection, seawater may be used (Aspelund et al.,
231 2006). However, using seawater to heat CO₂ implies losing energy that could otherwise be
232 recovered. For example, cold energy is already recovered from liquefied natural gas (Shi and
233 Che, 2009; Choi et al., 2013; Wang et al., 2013) and it can also be recovered for the cold CO₂
234 transported in ships. You et al. (2014) proposed to use a Rankine cycle between the CO₂
235 transported in ships and the injection conditions to produce electricity. They found that using
236 ammonia as the working fluid in the Rankine cycle yielded the best performance in terms of
237 power generation. The energy that can potentially be recovered in the heating process from
238 ship transport conditions to injection conditions is estimated to be $33.6 \cdot 10^6$ kWh for a mass
239 flow rate of 1 Mt/yr. The energy that could be effectively recovered by the Rankine cycle is

240 about $28.8 \cdot 10^6$ kWh for a mass flow rate of 1 Mt/yr (You et al., 2014), which is equivalent to
241 the mean electricity consumed by 5,780 people in the EU (Eurostat, 2016).

242

243 **4. CO₂ ALONG THE WELLBORE**

244 When injecting CO₂ along the injection well, CO₂ exchanges heat with the surrounding
245 rock (Brill and Mukherjee, 1999). Not only does this heat exchange influence the CO₂ flow
246 pattern inside the well, but also the surrounding rocks and well components are affected by
247 CO₂-induced temperature changes. CO₂ is heated as it flows downwards because of
248 compression and frictional forces, but usually at a lower rate than that of the geothermal
249 gradient (Lu and Connell, 2008; Luo and Bryant, 2010). Thus, CO₂ within the well is, in
250 general, colder than the rock, especially at high flow rates (Paterson et al., 2008; 2010). For
251 example, the CO₂ temperature at the bottom of the injection well at Cranfield, Mississippi,
252 increased by 16 °C when the mass flow rate was reduced by a factor of 4 (Luo et al., 2013),
253 showing that high flow rates of injection lead to lower injection temperatures. Another
254 representative example is the CO₂ injection at In Salah, Algeria, where CO₂ temperature at the
255 wellhead coincided with that of the surface temperature, but CO₂ reached the storage
256 formation at 1800 m deep 45 °C colder than the temperature corresponding to the geothermal
257 gradient (Bissell et al., 2011).

258 The lower temperature of CO₂ cools down the rock surrounding the well. But the heat
259 exchange between CO₂ and the surrounding rock is usually limited in time when a constant
260 mass flow rate is injected and thermal equilibrium may be reached within hours or a few days
261 (Lu and Connell, 2008). Once thermal equilibrium between CO₂ and the surrounding rock is
262 reached, adiabatic conditions occur within the injection well. Transient effects are sometimes
263 neglected to simplify calculation (Nimtz et al., 2010). However, heat exchange cannot be

264 neglected in the case of blowouts (Lindeberg, 2011) or if CO₂ injection is not continuous (Lu
265 and Connell, 2014a).

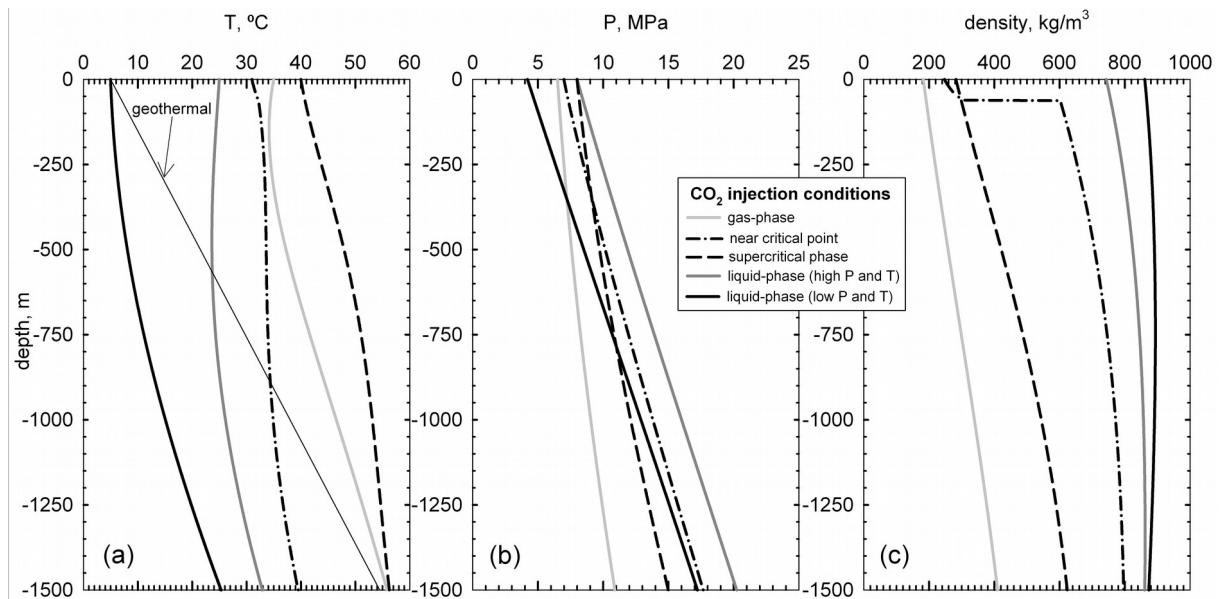
266 Current wellbore simulators, e.g., T2Well (Pan and Oldenburg, 2014), are capable of
267 handling transient effects. For instance, Lu and Connell (2014a) developed a transient non-
268 isothermal wellbore flow model for multispecies mixtures. Lu and Connell (2014a) found that
269 steady heat transfer models might be inappropriate for unsteady flows. Previous models based
270 on steady or quasi-steady flow models (e.g., Lu and Connell, 2008), partly or fully neglected
271 the effects of storage and inertial terms in the flow equations. This quasi-steady approach is
272 acceptable for injections of months or years, but not for unsteady conditions, e.g., non-
273 uniform flow rate. Lu and Connell (2014a) presented an example of Enhanced Coal Bed
274 Methane (ECBM). ECBM is a method to produce methane from coal beds by injecting CO₂,
275 which adsorbs in the coal, displacing methane. Lu and Connell (2014a) obtained a good
276 fitting of pressure and temperature at both the wellhead and bottomhole. CO₂ was injected in
277 liquid conditions from a tanker truck (at around 1.5 MPa and -30 °C, very close to the
278 saturation line), and two-phase flow conditions took place within the first meters of the well
279 due to partial vaporization of the liquid CO₂.

280 Another field test of CO₂ injection for ECBM purposes was carried out at Yuhbari,
281 Hokkaido, Japan, between 2003 and 2007 (Sasaki et al., 2009). The coal seam was at 900 m
282 deep, with a pressure and temperature of approximately 15.5 MPa and 28 °C, respectively.
283 Sasaki et al. (2009) found that coal permeability decreased up to a factor of 15 as the coal
284 became saturated in CO₂ due to swelling of coal. However, this swelling effect decreased for
285 successive injection experiments. Furthermore, the intrinsic permeability around the injection
286 well increased for successive injection experiments up to a factor of 6 due to fracturing of the
287 rock. CO₂ was injected at 68.5 °C, but CO₂ reached the bottom of the injection well in liquid
288 conditions, i.e., below 31.04 °C, due to heat loss along the injection well. The reason for such

289 high injection temperature was the intention to inject CO₂ in supercritical conditions rather
290 than in liquid state because the lower viscosity of supercritical CO₂ would facilitate CO₂
291 injection in such a low permeable formation. However, even insulating the injection tubing
292 was not enough to increase CO₂ temperature at low flow rates (4.5 ton/day). It was estimated
293 that to achieve supercritical conditions at the bottom of the injection well, a flow rate higher
294 than 12 t/day, i.e., 0.14 kg/s or 4380 t/yr, would be necessary.

295 These examples illustrate that pressure, temperature and density profiles along the wellbore
296 can be complex (Figure 2) and significantly vary for small changes in the pressure and
297 temperature at the wellhead (Vilarrasa et al., 2013). Since density depends on both pressure
298 and temperature, the system is strongly coupled and the CO₂ flow along the wellbore is not
299 trivial. This complexity is especially true when the injection conditions at the wellhead are
300 close to phase change (Lu and Connell, 2014b). For example, at Ketzin, Germany, CO₂ was
301 initially in gas state in the shallower 100 m of the well and in liquid state in the rest, but after
302 a transient period, two-phase flow conditions extended practically all along the well
303 (Henninges et al., 2011). Another example is that of Sleipner, Norway, where two-phase (gas
304 and liquid CO₂) conditions exist at the wellhead, the two-phase flow is maintained for the first
305 250 m of the injection well, but the phase that remains below the two-phase region can be
306 liquid instead of gas for slight changes in the wellhead conditions (Lindeberg, 2011).

307 To complicate the process even further, the pressure, temperature and density variation
308 with depth along the wellbore is also controlled by the overpressure induced at the storage
309 formation for a given flow rate. Thus, the resulting pressure and temperature conditions at the
310 wellhead will also depend on the injectivity of the storage formation. Therefore, wellbore
311 simulators should be coupled with reservoir simulators to properly model the CO₂ pressure
312 and temperature, which determines the density, along the injection well (Pan et al., 2011; Pan
313 and Oldenburg, 2014; Vilarrasa et al., 2013).



314

315 Figure 2. Non-isothermal flow of CO₂ through an injection well: temperature (a), pressure
 316 (b) and density (c) profiles. Comparison between different injection conditions at the
 317 wellhead (gas-, supercritical- and liquid-phase) (injection rate of 1.5 kg/s, geothermal
 318 gradient of 0.033 °C/m, well radius of 4.5 cm, overall heat transfer coefficient of 10 W m⁻²
 319 K⁻¹) (from Vilarrasa et al.,2013).

320

321 5. CO₂ STORAGE

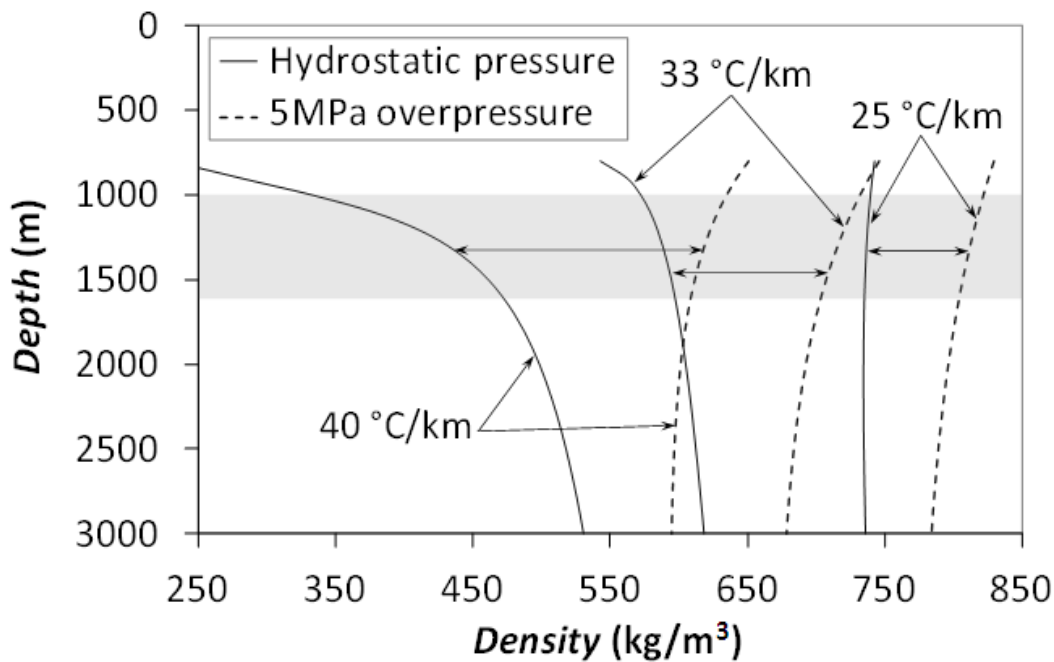
322 a. CO₂ INJECTION IN DEEP SEDIMENTARY FORMATIONS

323 CO₂ injection in deep saline formations induces temperature changes owing to processes
 324 such as Joule-Thomson cooling, endothermic water vaporization, exothermic CO₂ dissolution
 325 (Han et al., 2010; 2012) and because CO₂ will, most likely, reach the storage formation at a
 326 colder temperature than that corresponding to the geothermal gradient (Vilarrasa et al., 2014).
 327 When CO₂ enters into the storage formation, temperature slightly drops, by some decimals of
 328 degree, in the first tens of meters around the injection well, due to Joule-Thomson cooling as
 329 pressure drops with distance to the well (Han et al., 2010). The Joule-Thomson cooling effect
 330 may be more pronounced in depleted oil and gas fields due to the expansion of CO₂ when it

331 enters into the low pressure reservoir (Oldenburg, 2007; Pekot et al., 2011; Singh et al.,
332 2011a). However, the induced cooling is unlikely to cause injectivity problems due to hydrate
333 formation that could clog the well, except for initially cold reservoirs ($T < 20$ °C) (Mathias et
334 al., 2010; Ding and Liu, 2014). Apart from the Joule-Thomson cooling effect, water
335 vaporization into the dry CO₂ causes an additional cooling of around 1.0-2.0 °C. Water
336 vaporization only occurs in the vicinity of the injection well, within the first tens of meters in
337 the radial distance, because further away CO₂ becomes saturated with water. Outside the
338 vaporization front, temperature rises due to the exothermic CO₂ dissolution into the brine
339 (André et al., 2010; Han et al., 2010). The temperature increase due to CO₂ dissolution is of
340 around half degree and may be used for monitoring the advancement of the CO₂ plume
341 (Bielinski et al., 2008; Zhao and Cheng, 2014). Actually, a visible temperature signal can be
342 detectable upon CO₂ arrival at an observation well in the storage formation, as occurred at the
343 CO₂ injection pilot test sites of Frio, Texas (Hovorka et al., 2006) and Nagaoka, Japan (Sato et
344 al., 2009).

345 The dynamics of the CO₂ plume is governed, in part, by CO₂ density. While high CO₂
346 density leads to a viscous dominated flow, low CO₂ density yields gravity dominated CO₂
347 flow. CO₂ density depends on both pressure and temperature, which are not straightforward to
348 determine within the CO₂ plume, as shown by the existing uncertainty on the actual CO₂
349 density of the CO₂ plume at Sleipner, Norway (Nooner et al., 2007; Alnes et al., 2011).
350 Initially, pressure may be hydrostatic and predictable, but it may also vary significantly, such
351 as in depleted petroleum reservoirs. During CO₂ injection, an overpressure that is inversely
352 proportional to permeability is induced and thus, CO₂ density will increase with injection.
353 However, the range of CO₂ density change due to overpressure is limited, in general, to some
354 tens of kg/m³ (Figure 3). The geothermal gradient is also site dependent, which, for the depths
355 of storage, i.e., several km, may give rise to temperature variations of tens of degrees between

356 different storage sites (Randolph and Saar, 2011b). As a result, CO₂ density can vary several
 357 hundreds of kg/m³ from a storage site placed in a sedimentary basin with a high geothermal
 358 gradient to a site with a low geothermal gradient (Bachu, 2003) (Figure 3). The warmer the
 359 storage formation, the lower the CO₂ viscosity, which will facilitate flow and decrease
 360 overpressure (Wiese et al., 2010), but may enhance viscous fingering (Jackson et al., 2015).
 361 Temperature also affects the surface tension and the wetting angle, which play a role in
 362 capillarity (Singh et al., 2011b). The occurrence of these processes implies that it is important
 363 to account for non-isothermal effects even though CO₂ is injected in thermal equilibrium with
 364 the storage formation (Class et al., 2009).



365
 366 Figure 3. CO₂ density as a function of depth for several geothermal gradients at hydrostatic
 367 conditions and for a 5 MPa overpressure generated by CO₂ injection. Surface temperature
 368 is of 5, 10 and 15 °C for the geothermal gradients of 25, 33 and 40 °C/km, respectively. The
 369 shadowed region is the most appropriate depth interval for geologic carbon storage because
 370 it is deep enough to ensure a high CO₂ density that permits an efficient storage in terms of

371 volume, and also because deeper storage formations would imply higher drilling and
372 injection costs.

373 Thermal effects are more evident when the injected CO₂ is colder than the storage
374 formation. In such case, CO₂ cools down the rock around the wellbore, forming a cooler
375 region that tends to reach the same temperature as that of the inflowing CO₂ (Vilarrasa et al.,
376 2013). This cold region advances much behind of the desaturation front because CO₂ is heated
377 by the rock, which retards the advance of the cooling front with respect to the front of the CO₂
378 plume. The colder CO₂ is denser and more viscous than the supercritical CO₂ that is in
379 thermal equilibrium with the storage formation. Thus, viscous forces dominate in the cooled
380 region, leading to a steep CO₂ front that sweeps most of the thickness of the storage formation
381 (Rayward-Smith and Woods, 2011). However, as CO₂ warms up, its lower density and
382 viscosity leads to gravity override and thus, CO₂ tends to advance through the top portion of
383 the storage formation (Vilarrasa et al., 2014). The denser CO₂ in the cooled region occupies a
384 smaller volume than supercritical CO₂ and thus, displaces a smaller amount of brine, which
385 results in a slightly lower overpressure for cold CO₂ injection than for CO₂ in thermal
386 equilibrium with the storage formation (Vilarrasa et al., 2013; Randolph et al., 2013; Zhao and
387 Cheng, 2015). Furthermore, the cold region around the injection well remains for a long
388 period of time after the end of injection because the cooling front advances mainly by
389 advection of the cold CO₂ during injection, but the cooled rock is heated up by heat
390 conduction afterwards, which leads to a period to reach thermal equilibrium that is longer than
391 the injection period.

392

393 **b. THERMO-MECHANICAL EFFECTS**

394 CO₂ injection in deep saline formations implies temperature changes that will induce stress
395 and strain (Rutqvist, 2012). The region undergoing the largest temperature change will be

396 limited to a few hundreds of meters from the injection well for a CO₂ injection of several
397 decades. This region is relatively small compared to the extent of the CO₂ plume, which may
398 reach several kilometers (Vilarrasa et al., 2014). Still, thermal stresses may be a concern
399 (Celia et al., 2015) because CO₂ will, in general, reach the storage formation colder than the
400 rock, which may bring the stress state closer to failure conditions (de Simone et al., 2013).
401 Major faults will rarely be cooled down because injection wells will be placed far from them.
402 However, the thermal contraction of the rock around the injection well affects the stress field
403 in the far-field through deformations and associated stress-transfer and thus, the stability of
404 faults placed far away from the well may be reduced (Jeanne et al., 2014). This contraction of
405 the rock caused by cooling also leads to a smaller surface uplift induced by cold CO₂ injection
406 compared to CO₂ injection in thermal equilibrium with the storage formation (Goodarzi et al.,
407 2012; Fang et al., 2013). Furthermore, the lower portion of the caprock in the vicinity of
408 injection wells will be cooled down due to heat conduction once the cold CO₂ reaches the top
409 of the storage formation. This cooling may induce fracture instability within the caprock,
410 especially if the thermal expansion coefficients of the two formations are different (Vilarrasa
411 and Laloui, 2016).

412 Shear slip of fractures within the caprock and hydraulic fracture formation and propagation
413 across the caprock is, in principle, undesirable. However, in the presence of thick caprocks,
414 the overall caprock sealing capacity may not be compromised even though shear or tensile
415 failure conditions are reached at the bottom of the caprock, as demonstrated at In Salah,
416 Algeria. At this site, no leakage has occurred in spite of the fact that cooling probably
417 contributed to induce shear failure of the lower portion of the caprock (Vilarrasa et al., 2015).
418 Nevertheless, it is important to minimize the disturbance of the caprock integrity (Sagu and
419 Pao, 2013). Thus, thermal stresses should be accounted for to determine the maximum

420 sustainable injection pressure and maximum temperature drop that can be induced without
421 compromising the caprock integrity (Rutqvist et al., 2011; Kim and Hosseini, 2014b, 2015).

422 The distribution of thermal stresses is controlled by the extension of the cold region.
423 Analytical (Bao et al., 2014) and semi-analytical (LaForce et al., 2015) solutions have been
424 developed to estimate the position of the cold region and the induced thermal stresses. Even
425 though good estimates are obtained at the beginning of injection, when viscous forces
426 dominate and the CO₂ plume advances as a plug, differences arise as CO₂ moves away from
427 the injection well and gravity forces dominate, which leads to a cooling front that
428 preferentially advances along the top of the storage formation. Better estimates can be
429 obtained for the injection of brine with dissolved CO₂ because buoyancy forces are much
430 smaller than when a CO₂-rich phase is injected (Wu and Bryant, 2014). Nevertheless, this
431 thermo-hydro-mechanical coupled problem should be solved numerically to obtain accurate
432 solutions.

433 Numerical results are used to predict cooling-mediated hydraulic fracture initialization,
434 which occurs when the minimum effective stress exceeds the tensile strength of the rock
435 (Goodarzi et al., 2011, 2013; Luo and Bryant, 2011, 2013; Taylor and Bryant, 2014).
436 Hydraulic fractures, or shear slip of pre-existing fractures, may be beneficial if they are
437 confined within the storage formation because injectivity is enhanced (Goodarzi et al., 2010;
438 Rutqvist, 2012). Luo and Bryant (2014) modeled fracture propagation due to cooling in the
439 storage formation and found that stiff storage formations experience fast fracture growth,
440 leading to a low usage efficiency of the storage formation because the CO₂ plume becomes
441 elliptical as CO₂ advances preferentially along the hydraulic fracture. In contrast, soft storage
442 formations yield slow fracture propagation that may stop close to the well, giving rise to a
443 cylindrically-shaped CO₂ plume with high usage efficiency of the storage formation. Thus,
444 using thermal stresses properly can contribute to enhance the injectivity in the storage

445 formation. However, the propagation of hydraulic fractures or shear slip of pre-existing
446 fractures from the storage formation into the caprock should be avoided or, at least,
447 minimized to maintain the caprock sealing capacity. Apart from the magnitude of each stress
448 component and overpressure (Goodarzi et al., 2012; 2015), the propagation of shear or tensile
449 failure conditions from the storage formation into the caprock is controlled by several factors,
450 such as the stress regime, stress and strength heterogeneity between layers and the distance
451 from the injection well to the caprock.

452 Regarding the stress regime, strike slip stress regimes (i.e., stress states in which the
453 vertical stress is the intermediate principal stress) are more likely to propagate failure
454 conditions into the caprock than normal faulting (i.e., when the vertical stress is the maximum
455 principal stress) and reverse faulting stress regimes (i.e., when the vertical stress is the
456 minimum principal stress) (Vilarrasa, 2016). For example, simulation results of cold CO₂
457 injection at In Salah, Algeria, which is characterized by a strike slip stress regime, show that
458 the lower part of the caprock is likely to reach shear and tensile failure conditions (Preisig and
459 Prevost, 2011; Gor and Prévost, 2013; Gor et al., 2013; Vilarrasa et al., 2015). However, in
460 normal faulting stress regimes, failure conditions may not occur into the caprock even though
461 shear failure conditions are reached within the storage formation (Vilarrasa and Laloui, 2015).
462 This is because cooling of the storage formation induces a thermal stress reduction in all
463 directions, but since the overburden on top of the storage formation remains constant, a local
464 discontinuity in the vertical stress between the storage formation and the caprock appears
465 around the injection well. Therefore, stress redistribution occurs around the cooled region to
466 satisfy stress equilibrium and displacement compatibility. This stress redistribution causes the
467 horizontal total stresses of the lower portion of the caprock to increase, similar to an arch
468 effect, around the cooled region. The higher horizontal stresses tighten the caprock in a
469 normal faulting stress regime, improving its stability (Vilarrasa et al., 2013). A similar stress

470 redistribution occurs in a reverse faulting stress regime, but in this case, since the maximum
 471 principal stress is horizontal, the deviatoric stress increases in the caprock. However, due to
 472 the high confinement pressure, the decrease in stability is small, so fracture propagation
 473 across the caprock is unlikely. Only the caprock-reservoir and baserock-reservoir interfaces
 474 may reach failure conditions, but without propagating into the caprock (Bao et al., 2014).
 475 Furthermore, the stability within the storage formation may improve due to cooling in a
 476 reverse faulting stress regime, because, in the long-term, the horizontal stresses undergo a
 477 larger thermal stress reduction than the vertical stress, which decreases the deviatoric stress
 478 (Vilarrasa et al., 2014) (see Table 1 for a summary of the stress regime on rock stability
 479 changes induced by cooling).

480 Table 1. Thermo-mechanical effects of cooling on rock stability as a function of the stress
 481 regime

Stress regime	Storage formation	Caprock
Normal Faulting	Thermal stress reduction in both the maximum and the minimum principal stresses	Stress redistribution around the cooled region increases the minimum (horizontal) principal stress, reducing the deviatoric stress, which tightens the caprock
	brings the stress state closer to failure conditions	Stress redistribution around the cooled region affects equally the maximum (horizontal) and the minimum (horizontal) principal stresses, so the thermal stress reduction shifts the stress state closer to failure conditions maintaining the deviatoric stress

Reverse faulting

Stress redistribution around the cooled region increases the maximum (horizontal) principal stress, which increases the deviatoric stress, but just slightly due to the high confining stress

482

483 As far as the stress anisotropy between layers is concerned, caprocks are usually softer
484 than storage formations and thus, caprocks tend to accumulate less deviatoric stress than
485 storage formations as a result of tectonic plate movements (Hergert et al., 2015). This stress
486 heterogeneity between the storage formation and the caprock makes fracture propagation into
487 the caprock less likely. For example, Goodarzi et al. (2015) modeled the Ohio River Valley,
488 West Virginia, which is a strike slip stress regime, and therefore, thermal stresses are likely to
489 induce fracture propagation into the caprock, as may have occurred at In Salah, Algeria (Gor
490 et al., 2013; White et al., 2014). However, when accounting for the stress heterogeneity
491 between geological layers, hydraulic fractures may not propagate into the caprock because of
492 its higher minimum effective stress in normal faulting and strike slip stress regimes.
493 Furthermore, unlike in the storage formation, shear failure conditions may not be reached in
494 the caprock due to the lower deviatoric stress.

495 As for the position of the injection well with respect to the caprock, placing the well away
496 from the caprock may help to avoid inducing large thermal stresses in the caprock (Vilarrasa
497 et al., 2014). For example, Bonneville et al. (2014) used a 3D model with 4 horizontal wells to
498 simulate the CO₂ pilot site of FutureGen 2.0, Illinois. Tensile stresses were predicted at some
499 points close to the injection well when CO₂ was injected colder than the storage formation.
500 However, the top of the storage formation remained in compression because the cooling front
501 did not reach it during the simulation time. Nevertheless, the cooling front is likely to
502 eventually reach the caprock due to the buoyancy of CO₂. Yet, if the injection well is placed at

503 a certain distance from the caprock, the temperature drop will be smaller than at the injection
504 well, as occurred at Cranfield, Mississippi (Kim and Hosseini, 2014a; Luo et al., 2013).

505

506 **c. THERMO-GEOCHEMICAL PROCESSES**

507 One issue related to CO₂ injection in deep saline formations is salt precipitation around the
508 injection well (Pruess and Garcia, 2002). CO₂ will form a CO₂-rich region around the
509 injection well where liquid saturation will be reduced to the residual liquid saturation. CO₂
510 will be preferably injected dry, because if water is present, corrosion problems in pipes are
511 likely to occur. Thus, the residual brine will tend to evaporate into the dry CO₂, increasing the
512 salt concentration in the liquid phase (André et al., 2011). Once the equilibrium solubility is
513 reached, salt will precipitate, inducing crystallization pressure that might fracture the rock and
514 open new percolation pathways if stresses become high enough (Osselin et al., 2013). Salt
515 precipitation slightly decreases porosity. But since salt precipitates close to the pore throats,
516 the connectivity between the pores may clog, which could cause a dramatic decrease in
517 permeability and thus, in injectivity. Water evaporation increases at higher temperature
518 (Spycher and Pruess, 2005). Thus, a higher temperature generally results in more salt
519 precipitation (Kim et al., 2012). However, as brine is evaporated, the relative permeability to
520 CO₂ increases, which may partly compensate the permeability reduction due to salt
521 precipitation (Mathias et al., 2011).

522 Apart from salt precipitation, temperature affects the reaction rates of chemical reactions
523 (Song and Zhang, 2012). Geochemical reactions are more significant in carbonate rocks than
524 in siliciclastic rocks because carbonate minerals tend to dissolve in response to CO₂
525 dissolution into the brine, which gives rise to an acidic solution. The solubility of both CO₂
526 and carbonate rocks is higher at lower temperature. Thus, more CO₂ dissolution and carbonate
527 (mainly calcite and dolomite) dissolution will occur within the cold region that forms around

528 the injection well due to cold CO₂ injection. However, cooling has a minor effect on the
529 increment of the mineral volume fraction that is dissolved compared with CO₂ injection in
530 thermal equilibrium with the storage formation (Tutolo et al., 2015). The porosity
531 development around the injection well, which is the zone with the largest geochemical
532 changes, is small due to the low solubility of calcite (Saaltink et al., 2013). Thus, formation of
533 large cavities due to mineral dissolution should not be feared. If the temperature of the storage
534 formation is higher than 60 °C, dolomite precipitation is likely to occur, which may decrease
535 porosity and permeability. Consequently, cold CO₂ injection may inhibit precipitation of
536 carbonate minerals around the well in warm (>60 °C) storage formations and thus, injectivity
537 would not be negatively affected (André et al., 2010).

538 Geochemical reactions will lead to CO₂ mineral sequestration if carbon is fixed as
539 carbonate minerals. Carbon mineralization permits a permanent storage of CO₂ with
540 negligible leakage risk (Zevenhoven et al., 2011). This process is expected to occur in the
541 time scale of hundreds to thousands of years in deep saline aquifers (Zhang et al., 2009).
542 However, the mineralization process into carbonates can be dramatically speeded up in
543 basaltic rocks, with a 95 % mineralization of the injected CO₂ in less than 2 years (Matter et
544 al., 2016). Mineralization of CO₂ may also be achieved in industrial processes, such as steel
545 and iron-making slags. These chemical reactions release significant amounts of heat, which
546 could be useful in some industrial processes and affect reaction rates in geomaterials
547 (Zevenhoven et al., 2011).

548

549 **d. CARBON CAPTURE, UTILIZATION AND STORAGE**

550 Recently, it has been argued that CO₂ injection in deep saline aquifers should be
551 accompanied by its “utilization” to provide an added value that makes CCS an economically
552 feasible option for reducing CO₂ emissions to the atmosphere. Thus, CCS should evolve to

553 Carbon Capture, Utilization and Storage (CCUS). One of the most feasible options is
554 Enhanced Oil Recovery (EOR), which consists in injecting CO₂ in mature oil fields to
555 enhance their productivity (Brown et al., 2004; Hill et al., 2013). CO₂ is miscible in oil and
556 reduces oil viscosity, facilitating oil production. However, most of the injected CO₂ returns to
557 the surface dissolved into the produced oil. At surface, CO₂ is forced to exsolve from oil and
558 is reinjected. If more CO₂ is injected than produced, as it has been done at Weyburn, Canada,
559 since 2004 (Verdon et al., 2011), CO₂ storage takes place. Similarly, CO₂ can be used for
560 Enhanced Gas Recovery (EGR) in depleted gas fields, where the Joule-Thomson cooling
561 effect may be significant (Singh et al., 2012).

562 CO₂ can be stored in unminable coal seams, in which CO₂ displaces the methane originally
563 adsorbed to coal, leading to ECBM production (White et al., 2005). This CCUS option relies
564 on the higher affinity of CO₂ than methane to adsorb to coal. The potential storage capacity of
565 ECBM, though lower than that of saline aquifers, is large (Gale, 2004). The main limitation of
566 ECBM may be the relatively low permeability of coal seams. To overcome this drawback,
567 CO₂ may be injected quite warm, so that its viscosity is low and thus, overpressure does not
568 become large (Sasaki et al., 2009).

569 Other alternative CCUS options focus on using the geothermal energy of the deep
570 geological formations where CO₂ will be stored. One of the CO₂ storage methods that
571 involves geothermal energy recovery is the injection of CO₂ dissolved into brine (Pool et al.,
572 2013). Since brine with dissolved CO₂ is denser than brine without dissolved CO₂, CO₂-rich
573 brine tends to sink towards the bottom of the storage formation, making long-term CO₂
574 storage safe, especially in sloping aquifers. This storage concept has the drawback that brine
575 needs to be pumped and afterwards re-injected together with CO₂, which increases drilling
576 costs and pumping/compression costs. However, these additional costs may be offset by

577 recovering the geothermal energy of the pumped brine, which has a temperature higher than
578 that at the surface (Pool et al., 2013; Kervévan et al., 2014).

579 Another method for recovering geothermal energy consists in using CO₂ as the working
580 fluid (Randolph and Saar, 2011a). The thermosiphon concept using CO₂ as a circulating fluid
581 in heat pipes (Ochsner, 2008) was adopted as a means of geothermal energy, partly storing
582 CO₂ in deep geological formations (Freifeld et al., 2013; Buscheck et al., 2013; Adams et al.,
583 2014). Interestingly, CO₂ will circulate in the thermosiphon without the need of pumping (Pan
584 et al., 2015). Cold CO₂, and therefore dense, is injected in liquid conditions through a well
585 into a deep geologic formation. CO₂ will warm up as it moves away from the injection well,
586 becoming supercritical CO₂, and thus lighter (Vilarrasa et al., 2013). This supercritical CO₂
587 will flow upwards due to buoyancy through another well, returning to the surface, where it
588 will release its heat and electricity will be produced (Elliot et al., 2013). Apart from
589 minimizing the energy required for injection and pumping, CO₂ is more efficient than water as
590 a circulating fluid and yields higher power production (Adams et al., 2015). Once electricity
591 has been produced and the heat of CO₂ utilized, CO₂ cools down. Then, the cold CO₂ is
592 injected again into the injection well. Thus, the use of CO₂, instead of water, as the working
593 fluid, allows making use of geothermal energy without the need of mechanical pumping.
594 Furthermore, most of the injected CO₂ will remain deep underground, where it will be
595 permanently stored, and the economic benefit provided by the geothermal energy will convert
596 geologic carbon storage into a feasible option to mitigate climate change.

597

598 **6. CO₂ LEAKAGE THROUGH WELLS AND FAULTS**

599 CO₂ leakage is a concern in geologic carbon storage because: (i) the objective of keeping
600 CO₂ away from the atmosphere is not achieved (Hepple and Benson, 2005); (ii) freshwater
601 aquifers may undergo acidification and contamination (Lu et al., 2010; Trautz et al., 2012;

602 Ardelan and Steinnes, 2010); and (iii) asphyxiation hazard exists if CO₂ accumulates in
603 depressions on the land surface. CO₂ may leak from the storage formation across the caprock,
604 through faults or along wells. CO₂ leakage may be accompanied by brine leakage, which
605 could also be a concern if it reaches freshwater aquifers (Tillner et al., 2013). To prevent both
606 salinization of freshwater aquifers and CO₂ leakage from reaching the surface, multibarrier
607 systems, where saline aquifers alternate with low-permeability formations that serve as
608 caprocks, are an effective option (Birkholzer et al., 2009).

609 Natural analogues can provide useful information on the mechanisms that may promote
610 CO₂ leakage. Miocic et al. (2014) analyzed 49 natural CO₂ reservoirs, 10 of which were
611 known to leak. They found that leakage occurred either in shallow reservoirs, i.e., depths
612 shallower than 1000 m, where CO₂ was in gaseous phase, or in pressurized reservoirs where
613 the fracture gradient had been reached. The fact that reservoirs with gaseous CO₂ are more
614 prone to leak than reservoirs containing supercritical CO₂ is probably due to the higher
615 buoyancy of the less dense gaseous CO₂. On the other hand, reservoirs that are
616 underpressurized with respect to the overburden are less likely to leak than reservoirs that are
617 overpressurized with respect to the overburden. However, in geologic carbon storage, this
618 factor will generally not be favorable due to the overpressure induced by CO₂ injection.
619 Though it has been proposed by Réveillère and Rohmer (2011) and Réveillère et al. (2012) to
620 inject brine into the caprock to create a hydraulic barrier against CO₂ leakage, this injection
621 could jeopardize the caprock integrity because fluid injection in the caprock would
622 significantly increase pore pressure due to the low-permeability of the caprock. This pressure
623 buildup would reduce the effective stresses and failure conditions could be reached, which
624 could cause the opposite effect as the pursued one.

625 Unlike caprocks, which are likely to remain stable (Vilarrasa and Carrera, 2015), wellbores
626 are the most likely conduit for CO₂ to escape from the storage formation, especially in

627 sedimentary basins where hydrocarbons have been produced. A clear example of the potential
628 effect of wellbores in hydrocarbon basins on CO₂ leakage is the Alberta Basin, Canada, which
629 has more than 300,000 wells in 900,000 km² (Gasda et al., 2004). Some of the wellbore
630 simulators used for calculating CO₂ injection along the injection well (recall Section 4) can
631 also be used for calculating non-isothermal CO₂ leakage just by adding a few modifications
632 (Pan et al., 2011; Pan and Oldenburg, 2014). Furthermore, some efforts have been made to
633 explain CO₂ leakage through wells analytically (e.g., Nordbotten et al., 2004, 2005). However,
634 the thermal effects that occur during CO₂ leakage make it very complicated to develop
635 analytical or semi-analytical solutions that give good estimates of CO₂ leakage along
636 abandoned wells. To illustrate this, Ebigbo et al. (2007) compared the semi-analytical
637 solutions of Nordbotten et al. (2004, 2005) for leaky wells with numerical solutions. Ebigbo et
638 al. (2007) found that the semi-analytical solutions compare well with the numerical
639 simulations when the simplifying assumptions of the semi-analytical solution, which include
640 isothermal conditions, are taken into account in the numerical model. However, as the
641 simplifying assumptions are relaxed, numerical results increasingly differ from those of the
642 semi-analytical solution. In particular, the semi-analytical solution fails to give good results
643 when non-isothermal effects occur. This limitation was revealed by a model in which CO₂
644 changes from liquid to gas inside of a leaky well that connects two aquifers between 800 and
645 640 m deep, which gives rise to a 1.5 °C drop at the top of the leaky well (depth of 640 m) due
646 to the phase change.

647 The CO₂ dynamics in a leaky well can be very diverse. Initially, the wellbore is saturated
648 with water. Once CO₂ starts leaking, water is initially displaced upwards due to the buoyancy
649 of CO₂. As CO₂ advances upwards, CO₂ saturation increases due to gas exsolution as pressure
650 decreases at shallower depths and, due to the lower density of gaseous than supercritical CO₂
651 (Pan et al., 2009). This phase change occurs when the pressure becomes lower than the critical

652 CO₂ pressure of 7.4 MPa, i.e., at depths lower than about 800 m. If the amount of available
653 CO₂ for leaking into the well is unlimited, a quasi-steady state is rapidly reached, within 30
654 minutes (Pan et al., 2011). The temperature profile stabilizes when the steady state flow is
655 reached. But before this stabilization occurs, the temperature profile along the well reaches a
656 maximum due to CO₂ dissolution into the water, which is an exothermic reaction, followed by
657 a local minimum caused by CO₂ expansion. However, in general, CO₂ mobility in the
658 reservoir controls the leakage rate through an open borehole and therefore, CO₂ availability
659 will usually be limited. In particular, if the CO₂ saturation is close to the residual gas
660 saturation, CO₂ cannot continuously flow through the wellbore, leading to a geyser like
661 leakage (Pan et al., 2011). Furthermore, in closed reservoirs, CO₂ leakage induces a reduction
662 of the reservoir pressure, which causes a progressive reduction of CO₂ leakage rate.

663 In the scenarios modeled by Pan et al. (2009; 2011), CO₂ transitioned from supercritical to
664 gas without undergoing any phase change. This may be the case in the presence of high
665 geothermal gradient. However, liquid CO₂ may appear due to the cooling that occurs during
666 expansion when considering a broader range of geothermal gradients or for insulated wells
667 that receive very limited heat from the surrounding rock (Oldenburg et al., 2012). Long-term
668 CO₂ leakage may also lead to a similar situation than that of an insulated well once the
669 surrounding rock is cooled down and provides a low amount of heat to CO₂. If liquid CO₂
670 forms, the saturation line is eventually reached at a certain depth, where liquid and gas will
671 coexist. The depth interval where liquid and gas CO₂ coexist experiences strong non-
672 isothermal effects due to the Joule-Thomson effect (Burnett, 1923; Charnley et al., 1955) that
673 occurs as a result of the expansion that takes place when liquid CO₂ boils into subcritical
674 gaseous CO₂ (Pruess, 2011). This cooling results in an advance, mainly upwards, of the depth
675 interval where CO₂ stays on the saturation line (Oldenburg et al., 2012). Thus, the temperature
676 difference (cooling) with respect to the geothermal gradient becomes larger as the two-phase

677 conditions advance upwards. In extreme cases, CO₂ release in wells may lead to pressure and
678 temperatures at the wellhead close to those of the triple point (i.e., 0.511 MPa and -56.35 °C,
679 respectively). If such conditions are reached, CO₂ will be ejected as solid “dry ice” particles,
680 as has already occurred in EOR fields (Skinner, 2003). Similar processes would occur if CO₂
681 leakage occurs through a fault instead than through a well.

682 If CO₂ leaks through a fault or fracture, brine will start leaking before CO₂ (Rutqvist and
683 Tsang, 2002), which will induce a temperature increase along the fracture due to the warmer
684 temperature of the upwards flowing brine (Zeidouni et al., 2014). But the leaking CO₂, which
685 is in supercritical conditions at the storage formation from which CO₂ leaks, may change to
686 liquid conditions as it leaks upwards through a fault (Pruess, 2005a). Simulation results of
687 Pruess (2005a) show that liquid CO₂ boils into gas at around 630 m because at this depth the
688 pressure and temperature of CO₂ are such that they lie on the saturation line. The phase
689 change from liquid to gas is accompanied by a large increase in volume, i.e., a large density
690 decrease, and a decrease in viscosity. As a result of CO₂ depressurization and expansion as it
691 migrates towards shallower depths, temperature will decrease due to the Joule-Thomson
692 cooling effect. Furthermore, temperature will drop because latent heat is absorbed by the
693 phase change process. The region where CO₂ changes its phase from liquid to gas becomes a
694 3-phase region because there is water present (Pruess, 2005b). Mobility is significantly
695 reduced in this region, which hinders CO₂ upflow locally and promotes lateral spreading of
696 CO₂. The decrease in CO₂ flow causes the temperature to increase again due to heat
697 conduction from the surrounding rock, increasing the temperature and eventually recovering a
698 two-phase flow that allows upward CO₂ flow again. This leads to a quasi-periodic discharge
699 of CO₂ towards the surface that shows a tendency to increase its period with time. Pruess
700 (2005a) also performed a simulation in which temperature was artificially maintained constant
701 by specifying very large rock specific heat. A constant temperature led to a monotonic

702 increase of leakage fluxes with time, also observed in an isothermal numerical simulation
703 performed by Pruess and Garcia (2002), without the formation of the 3-phase region. This
704 difference allowed Pruess (2005a) to conclude that the availability of conductive heat transfer
705 is the limiting factor of the growth of CO₂ fluxes when non-isothermal effects are taken into
706 account.

707 Simulation results show that the strong dependency of the CO₂ properties on pressure and
708 temperature leads to complex processes that can have either positive or negative feedback on
709 the CO₂ leakage rates. The decrease in both CO₂ density and viscosity as CO₂ migrates
710 upwards provides a self-enhancement of the leakage rate. However, strong cooling caused by
711 phase change from liquid to gaseous CO₂ may cause three-phase flow that self-limits leakage
712 and may give rise to geysering (e.g., Pruess, 2008). Since thermal effects play a relevant role
713 in CO₂ leakage processes, measuring temperature along wells can be useful to detect leakage.

714 The temperature signal can be used to detect not only CO₂ leakage, but also brine leakage.
715 If brine leakage occurs, temperature will increase because of the warmer temperature of the
716 brine that comes from deeper depths. But if brine leakage is followed by CO₂ leakage, cooling
717 will take place once CO₂ reaches a certain depth due to CO₂ expansion. The main drawback of
718 leakage detection using temperature signals is that the leakage-induced temperature changes
719 cover a small volume around the leakage pathway, which makes it difficult to detect unless
720 the monitoring well is very close to where leakage occurs (Tao et al., 2013). In contrast, the
721 pressure signal extends rapidly over large distances, but increases regardless of the fluid that
722 is leaking. Thus, a combination of pressure with temperature monitoring is recommendable,
723 because pressure monitoring can detect pressure perturbations which origin is located far
724 away from the measurement point and if the temperature measurements are close to leakage,
725 information on the leaking fluid can be obtained (Hurter et al., 2007).

726 Underground temperature and pressure monitoring can be combined with deformation
727 measurements to detect leakage because deformation spreads instantaneously in response to
728 overpressure (Rutqvist, 2012). Surface uplift evolution can be measured with InSAR, as it
729 was successfully done at In Salah, Algeria (Vasco et al., 2008). Even though deformation
730 measurements do not directly inform about thermal effects, their interpretation using coupled
731 thermo-hydro-mechanical numerical simulations may allow determining the extension of the
732 cooled region around injection wells because the contraction of the rock induced by cooling
733 reduces the magnitude of the surface uplift (Goodarzi et al., 2015).

734 Temperature can be monitored using point measurements, wireline-deployed instruments
735 or fiber-optic distributed temperature sensing (DTS) cables (Reinsch et al., 2013; Nuñez-
736 Lopez et al., 2014). The wireline-deployed instruments provide logs of temperature as a
737 function of depth and the DTS produces continuous temperature measurements both in time
738 and space along the cable. DTS can provide, after careful calibration, resolution and accuracy
739 as small as 0.02 and 0.3 °C, respectively, as reported for a gas-hydrate monitoring application
740 at around 1,200 m deep (Henninges et al., 2005). Hoang et al. (2011) used DTS to infer the
741 productive zones after hydraulic fracturing operations from temperature measurements
742 outside of the well. Concerning geologic carbon storage, temperature measurements have
743 already been performed at CO₂ pilot test sites, like Frio, Texas (Hovorka et al., 2006) and
744 industrial scale sites, like Cranfield, Mississippi (Hovorka et al., 2013).

745

746 **7. RESEARCH GAPS AND CHALLENGES**

747 Based on the review of thermal effects on geologic carbon storage, a series of research
748 gaps and challenges have been identified. The following list suggests future research lines to
749 address them:

750 - The effect of impurities on corrosion of pipelines needs to be better understood.
751 Pipeline corrosion may lead to the failure of pipelines and thus, it is crucial to develop
752 guidelines for the metal requirements of pipelines depending on the flue gas composition.
753 These guidelines should take into account the possibility of strong cooling caused by
754 expansion of CO₂ if normal operation is interrupted suddenly.

755 - The connection between CO₂ transport and injection into the well is still associated
756 with significant uncertainties. Huge amounts of energy can be saved, and even generated, by
757 employing smart ways of using the high pressure at which liquid CO₂ is transported through
758 pipelines.

759 - Wellbore and reservoir simulators are usually decoupled. However, the pressure and
760 temperature at the bottom of the injection well should coincide with those in the storage
761 formation at the injection well. Coupling these two simulators will permit obtaining realistic
762 injection conditions that could be used to optimize the pressure and temperature at the
763 wellhead.

764 - The thermo-mechanical effects of cold CO₂ injection have not been widely
765 investigated and are not fully understood. In particular, different studies on caprock stability
766 due to cooling give results that are not in full agreement. Thus, the processes that govern
767 caprock stability are still not well-known and further investigation is required.

768 - The effect of geochemical reactions (dissolution/precipitation) on the geomechanical
769 properties and responses of different rock types has not been addressed in detail. The
770 combined work of geochemist with geomechanical experts is required to shed light on this
771 coupled effect.

772 - Coupled thermo-hydro-mechanical-chemical processes have not been investigated yet
773 in detail due to the high complexity of this problem that involves extremely high

774 computational cost. To address this coupled problem, more efficient numerical simulators are
775 required.

776 - Further investigation is needed to understand three-phase (water, gaseous CO₂ and
777 liquid CO₂) relative permeability and hysteresis. Three-phase may form in CO₂ leakage
778 pathways and may lead to a self-limiting feedback that decreases the leakage rate. However,
779 the capillary properties of three-phase flow are not well-known.

780 - The geomechanical implications of CO₂ leakage related to cooling effects, especially
781 when liquid CO₂ is formed, have not been investigated yet.

782 - CCUS: one of the main barriers to put in practice CCS is its elevated cost. To reduce
783 its cost, adding a “utilization” that provides an economic benefit is highly recommendable.
784 More efforts should be devoted to develop CCUS options.

785 - Finally, to achieve a successful deployment of CCS and CCUS, there should be a
786 transition from pilot to demonstration scale sites. The Boundary Dam Carbon Capture Project,
787 in Saskatchewan, Canada, has been the first commercial-scale CCS project. This is a great
788 first start, but it should be followed by many other industrial scale projects.

789

790 **ACKNOWLEDGMENTS**

791 V.V. acknowledges financial support from the “TRUST” project (European Community's
792 Seventh Framework Programme FP7/2007-2013 under grant agreement n 309607) and from
793 “FracRisk” project (European Community's Horizon 2020 Framework Programme H2020-
794 EU.3.3.2.3 under grant agreement n 640979). This work was funded in part by the Assistant
795 Secretary for Fossil Energy, National Energy Technology Laboratory, National Risk
796 Assessment Partnership, of the U.S. Department of Energy under Contract No. DEAC02-
797 05CH11231.

798

799 **REFERENCES**

- 800 Adams, B. M., Kuehn, T. H., Bielicki, J. M., Randolph, J. B., & Saar, M. O. (2014). On the
801 importance of the thermosiphon effect in CPG (CO₂ plume geothermal) power systems.
802 *Energy*, 69, 409-418.
- 803 Adams, B. M., Kuehn, T. H., Bielicki, J. M., Randolph, J. B., & Saar, M. O. (2015). A
804 comparison of electric power output of CO₂ Plume Geothermal (CPG) and brine
805 geothermal systems for varying reservoir conditions. *Applied Energy*, 140, 365-377.
- 806 Alnes, H., Eiken, O., Nooner, S., Sasagawa, G., Stenvold, T., & Zumberge, M. (2011). Results
807 from Sleipner gravity monitoring: updated density and temperature distribution of the CO₂
808 plume. *Energy Procedia*, 4, 5504-5511.
- 809 André, L., Azaroual, M., Peysson, Y., & Bazin, B. (2011). Impact of porous medium
810 desiccation during anhydrous CO₂ injection in deep saline aquifers: Up scaling from
811 experimental results at laboratory scale to near-well region. *Energy Procedia*, 4, 4442-
812 4449.
- 813 André, L., Azaroual, M., & Menjot, A. (2010). Numerical simulations of the thermal impact
814 of supercritical CO₂ injection on chemical reactivity in a carbonate saline reservoir.
815 *Transport in porous media*, 82(1), 247-274.
- 816 Ardelan, M. V., & Steinnes, E. (2010). Changes in mobility and solubility of the redox
817 sensitive metals Fe, Mn and Co at the seawater-sediment interface following CO₂ seepage.
818 *Biogeosciences*, 7(2), 569-583.
- 819 Aspelund, A., Mølnvik, M. J., & De Koeijer, G. (2006). Ship Transport of CO₂: Technical
820 Solutions and Analysis of Costs, Energy Utilization, Exergy Efficiency and CO₂ Emissions.
821 *Chemical Engineering Research and Design*, 84(9), 847-855.
- 822 Bachu, S. (2003). Screening and ranking of sedimentary basins for sequestration of CO₂ in
823 geological media in response to climate change. *Environmental Geology*, 44(3), 277-289.

824 Bao, J., Xu, Z., & Fang, Y. (2014). A coupled thermal-hydro-mechanical simulation for
825 carbon dioxide sequestration. *Environmental Geotechnics*, doi: 10.1680/envgeo.14.00002.

826 Baxter, P. J., Baubron, J. C., & Coutinho, R. (1999). Health hazards and disaster potential of
827 ground gas emissions at Furnas volcano, Sao Miguel, Azores. *Journal of Volcanology and*
828 *Geothermal Research*, 92(1), 95-106.

829 Bielinski, A., Kopp, A., Schütt, H., & Class, H. (2008). Monitoring of CO₂ plumes during
830 storage in geological formations using temperature signals: Numerical investigation.
831 *International Journal of Greenhouse Gas Control*, 2(3), 319-328.

832 Birkholzer, J. T., Zhou, Q., & Tsang, C. F. (2009). Large-scale impact of CO₂ storage in deep
833 saline aquifers: a sensitivity study on pressure response in stratified systems. *International*
834 *Journal of Greenhouse Gas Control*, 3(2), 181-194.

835 Bissell, R. C., Vasco, D. W., Atbi, M., Hamdani, M., Okwelegbe, M., & Goldwater, M. H.
836 (2011). A full field simulation of the In Salah gas production and CO₂ storage project
837 using a coupled geo-mechanical and thermal fluid flow simulator. *Energy Procedia*, 4,
838 3290-3297.

839 Bonneville, A., Nguyen, B. N., Stewart, M., Hou, Z. J., Murray, C., & Gilmore, T. (2014).
840 Geomechanical evaluation of thermal impact of injected CO₂ temperature on a geological
841 reservoir: application to the FutureGen 2.0 Site. *Energy Procedia*, 63, 3298-3304.

842 Böttcher, N., Taron, J., Kolditz, O., Park, C. H., & Liedl, R. (2012). Evaluation of thermal
843 equations of state for CO₂ in numerical simulations. *Environmental Earth Sciences*, 67(2),
844 481-495.

845 Brill, J., Mukherjee, H., (1999). *Multiphase Flow in Wells*. Henry L. Doherty Memorial Fund
846 of AIME, Society of Petroleum Engineers Inc., Richardson, TX.

847 Brown, G., Carvalho, V., Wray, A., Smith, D., Toombs, M., & Pennell, S. (2004). Monitoring
848 alternating CO₂ and water injection and its effect on production in a carbonate reservoir

849 using permanent fiber-optic distributed temperature systems. In *SPE Annual Technical*
850 *Conference and Exhibition*, Houston, Texas, 26–29 September 2004.

851 Burnett, E. S. (1923). Experimental study of the Joule-Thomson effect in carbon dioxide.
852 *Physical Review*, 22(6), 590.

853 Buscheck, T. A., Elliot, T. R., Celia, M. A., Chen, M., Sun, Y., Hao, Y., Lu, C., Wolery, T. J. &
854 Aines, R. D. (2013). Integrated geothermal-CO₂ reservoir systems: reducing carbon
855 intensity through sustainable energy production and secure CO₂ storage. *Energy Procedia*,
856 37, 6587-6594.

857 Celia, M. A., Bachu, S., Nordbotten, J. M., & Bandilla, K. W. (2015). Status of CO₂ storage in
858 deep saline aquifers with emphasis on modeling approaches and practical simulations.
859 *Water Resources Research*, 51(9), 6846-6892.

860 Charnley, A., Rowlinson, J. S., Sutton, J. R., & Townley, J. R. (1955). The isothermal Joule-
861 Thomson coefficient of some binary gas mixtures. *Proceedings of the Royal Society of*
862 *London. Series A. Mathematical and Physical Sciences*, 230(1182), 354-358.

863 Choi, I. H., Lee, S., Seo, Y., & Chang, D. (2013). Analysis and optimization of cascade
864 Rankine cycle for liquefied natural gas cold energy recovery. *Energy*, 61, 179-195.

865 Class, H., Ebigbo, A., Helmig, R., Dahle, H. K., Nordbotten, J. M., Celia, M. A., Audigane, P.,
866 Darcis, M., Ennis-King, J., Fan, Y., Flemisch, B., Gasda, S. E., Jin, M., Krug, S.,
867 Labregere, D., Beni, A. N., Pawar, R. J., Sbai, A., Thomas, S. G., Trenty, L., & Wei, L.
868 (2009). A benchmark study on problems related to CO₂ storage in geologic formations.
869 *Computational Geosciences*, 13(4), 409-434.

870 de Simone, S., Vilarrasa, V., Carrera, J., Alcolea, A., & Meier, P. (2013). Thermal coupling
871 may control mechanical stability of geothermal reservoirs during cold water injection.
872 *Physics and Chemistry of the Earth, Parts A/B/C*, 64, 117-126.

873 Ding, T., & Liu, Y. (2014). Simulations and analysis of hydrate formation during CO₂
874 injection into cold saline aquifers. *Energy Procedia*, 63, 3030-3040.

875 Duan, Z., & Sun, R. (2003). An improved model calculating CO₂ solubility in pure water and
876 aqueous NaCl solutions from 273 to 533 K and from 0 to 2000 bar. *Chemical geology*,
877 193(3), 257-271.

878 Ebigbo, A., Class, H., & Helmig, R. (2007). CO₂ leakage through an abandoned well:
879 problem-oriented benchmarks. *Computational Geosciences*, 11(2), 103-115.

880 Elliot, T. R., Buscheck, T. A., & Celia, M. (2013). Active CO₂ reservoir management for
881 sustainable geothermal energy extraction and reduced leakage. *Greenhouse Gases: Science
882 and Technology*, 3(1), 50-65.

883 Eurostat (2016). Consumption of Energy. [ec.europa.eu/eurostat/statistics-](http://ec.europa.eu/eurostat/statistics-explained/index.php/Consumption_of_energy)
884 [explained/index.php/Consumption_of_energy](http://ec.europa.eu/eurostat/statistics-explained/index.php/Consumption_of_energy). Consulted on July 25, 2016.

885 Fang, Y., Nguyen, B. N., Carroll, K., Xu, Z., Yabusaki, S. B., Scheibe, T. D., & Bonneville, A.
886 (2013). Development of a coupled thermo-hydro-mechanical model in discontinuous
887 media for carbon sequestration. *International Journal of Rock Mechanics and Mining
888 Sciences*, 62, 138-147.

889 Freifeld, B., Zakim, S., Pan, L., Cutright, B., Sheu, M., Doughty, C., & Held, T. (2013).
890 Geothermal energy production coupled with CCS: a field demonstration at the SECARB
891 Cranfield Site, Cranfield, Mississippi, USA. *Energy Procedia*, 37, 6595-6603.

892 Gale, J., & Davison, J. (2004). Transmission of CO₂—safety and economic considerations.
893 *Energy*, 29(9), 1319-1328.

894 Gale, J., (2004). Geological storage of CO₂: What do we know, where are the gaps and what
895 more needs to be done? *Energy* 29, 1329-1338.

896 Gasda, S. E., Bachu, S., & Celia, M. A. (2004). Spatial characterization of the location of
897 potentially leaky wells penetrating a deep saline aquifer in a mature sedimentary basin.
898 *Environmental geology*, 46(6-7), 707-720.

899 Ghassemi, A., Tarasovs, S., & Cheng, A. D. (2007). A 3-D study of the effects of
900 thermomechanical loads on fracture slip in enhanced geothermal reservoirs. *International*
901 *Journal of Rock Mechanics and Mining Sciences*, 44(8), 1132-1148.

902 Goodarzi, S., Settari, A., Zoback, M. D., & Keith, D. (2010). Thermal aspects of
903 geomechanics and induced fracturing in CO₂ injection with application to CO₂
904 sequestration in Ohio River Valley. In *SPE International Conference on CO₂ Capture,*
905 *Storage, and Utilization*. New Orleans, Louisiana, 10-12 November 2010.

906 Goodarzi, S., Settari, A., & Keith, D. (2011). Geomechanical modeling for CO₂ storage in
907 Wabamun Lake Area of Alberta, Canada. *Energy Procedia*, 4, 3399-3406.

908 Goodarzi, S., Settari, A., & Keith, D. (2012). Geomechanical modeling for CO₂ storage in
909 Nisku aquifer in Wabamun Lake area in Canada. *International Journal of Greenhouse Gas*
910 *Control*, 10, 113-122.

911 Goodarzi, S., Settari, A., Zoback, M., & Keith, D. W. (2013). Thermal effects on shear
912 fracturing and injectivity during CO₂ storage. In *ISRM International Conference for*
913 *Effective and Sustainable Hydraulic Fracturing*, Brisbane, Australia, 20-22 May 2013.

914 Goodarzi, S., Settari, A., Zoback, M.D., & Keith, D.W. (2015). Optimization of a CO₂ storage
915 project based on thermal, geomechanical and induced fracturing effects. *Journal of*
916 *Petroleum Science and Engineering*, 134, 49-59.

917 Gor, G. Y., Elliot, T. R., & Prévost, J. H. (2013). Effects of thermal stresses on caprock
918 integrity during CO₂ storage. *International Journal of Greenhouse Gas Control*, 12, 300-
919 309.

920 Gor, G. Y., & Prévost, J. H. (2013). Effect of CO₂ Injection Temperature on Caprock Stability.
921 *Energy Procedia*, 37, 3727-3732.

922 Han, W. S., Stillman, G. A., Lu, M., Lu, C., McPherson, B. J., & Park, E. (2010). Evaluation
923 of potential nonisothermal processes and heat transport during CO₂ sequestration. *Journal*
924 *of Geophysical Research: Solid Earth (1978–2012)*, 115(B7).

925 Han, W. S., Kim, K. Y., Park, E., McPherson, B. J., Lee, S. Y., & Park, M. H. (2012).
926 Modeling of spatiotemporal thermal response to CO₂ injection in saline formations:
927 Interpretation for monitoring. *Transport in porous media*, 93(3), 381-399.

928 Hansen, O., Gilding, D., Nazarian, B., Osdal, B., Ringrose, P., Kristoffersen, J. B., Eiken, O.
929 & Hansen, H. (2013). Snøhvit: the history of injecting and storing 1 Mt CO₂ in the Fluvial
930 Tubåen Fm. *Energy Procedia*, 37, 3565-3573.

931 Harvey, A. H. (1996). Semiempirical correlation for Henry's constants over large temperature
932 ranges. *AIChE journal*, 42(5), 1491-1494.

933 Hennings, J., Huenges, E., & Burkhardt, H. (2005). In situ thermal conductivity of gas-
934 hydrate-bearing sediments of the Mallik 5L-38 well. *Journal of Geophysical Research:*
935 *Solid Earth (1978–2012)*, 110(B11).

936 Hennings, J., Liebscher, A., Bannach, A., Brandt, W., Hurter, S., Köhler, S., Möller, F. &
937 CO2SINK Group. (2011). PT- ρ and two-phase fluid conditions with inverted density
938 profile in observation wells at the CO₂ storage site at Ketzin (Germany). *Energy Procedia*,
939 4, 6085-6090.

940 Hepple, R. P., & Benson, S. M. (2005). Geologic storage of carbon dioxide as a climate
941 change mitigation strategy: performance requirements and the implications of surface
942 seepage. *Environmental Geology*, 47(4), 576-585.

943 Hergert, T., Heidbach, O., Reiter, K., Giber, S.B. & Marschall, P. (2015). Stress field
944 sensitivity analysis in a sedimentary sequence of the Alpine foreland, northern Switzerland.
945 *Solid Earth*, 6, 533-552.

946 Hill, B., Hovorka, S., & Melzer, S. (2013). Geologic carbon storage through enhanced oil
947 recovery. *Energy Procedia*, 37, 6808-6830.

948 Hoang, H., Mahadevan, J., & Lopez, H. D. (2011). Interpretation of wellbore temperatures
949 measured using distributed temperature sensors during hydraulic fracturing. In *SPE*
950 *Hydraulic Fracturing Technology Conference*. Society of Petroleum Engineers.

951 Hovorka, S. D., Benson, S. M., Doughty, C., Freifeld, B. M., Sakurai, S., Daley, T. M.,
952 Kharaka, Y. K., Holtz, M. H., Trautz, R. C., Nance, H. S., Myer, L. R., & Knauss, K. G.
953 (2006). Measuring permanence of CO₂ storage in saline formations: the Frio experiment.
954 *Environmental Geosciences*, 13(2), 105-121.

955 Hovorka, S. D., Meckel, T. A., & Treviño, R. H. (2013). Monitoring a large-volume injection
956 at Cranfield, Mississippi—project design and recommendations. *International Journal of*
957 *Greenhouse Gas Control*, 18, 345-360.

958 Hurter, S., Garnett, A. A., Bielinski, A., & Kopp, A. (2007). Thermal signature of free-phase
959 CO₂ in porous rocks: detectability of CO₂ by temperature logging. *SPE Offshore Europe*,
960 SPE 109007, Aberdeen, Scotland, UK, 4-7 September.

961 IEAGHG (2013). CO₂ pipeline infrastructure. Report 2013/18.

962 IPCC (Intergovernmental Panel on Climate Change) (2005). In: Metz, B., Davidson, O., de
963 Coninck, H.C., Loos, M. & Mayer, L.A. (eds). Special report on carbon dioxide capture
964 and storage. Cambridge University Press, Cambridge.

965 Jackson, S. J., Stevens, D., Giddings, D., & Power, H. (2015). Dynamic-wetting effects in
966 finite-mobility-ratio Hele-Shaw flow. *Physical Review E*, 92(2), 023021.

967 Jeanne, P., Rutqvist, J., Dobson, P. F., Walters, M., Hartline, C., & Garcia, J. (2014). The
968 impacts of mechanical stress transfers caused by hydromechanical and thermal processes
969 on fault stability during hydraulic stimulation in a deep geothermal reservoir. *International*
970 *Journal of Rock Mechanics and Mining Sciences*, 72, 149-163.

971 Kaldal, G. S., Jónsson, M. Þ., Pálsson, H., & Karlsdóttir, S. N. (2015). Structural Analysis of
972 Casings in High Temperature Geothermal Wells in Iceland. *Proceedings of World*
973 *Geothermal Congress 2015*, Melbourne, Australia, 19-25 April 2015.

974 Kervévan, C., Beddelem, M. H., & O'Neil, K. (2014). CO₂-DISSOLVED: a Novel Concept
975 Coupling Geological Storage of Dissolved CO₂ and Geothermal Heat Recovery–Part 1:
976 Assessment of the Integration of an Innovative Low-cost, Water-based CO₂ Capture
977 Technology. *Energy Procedia*, 63, 4508-4518.

978 Kim, K. Y., Han, W. S., Oh, J., Kim, T., & Kim, J. C. (2012). Characteristics of salt-
979 precipitation and the associated pressure build-up during CO₂ storage in saline aquifers.
980 *Transport in porous media*, 92(2), 397-418.

981 Kim, S., & Hosseini, S. A. (2014a). Above-zone pressure monitoring and geomechanical
982 analyses for a field-scale CO₂ injection project in Cranfield, MS. *Greenhouse Gases:*
983 *Science and Technology*, 4(1), 81-98.

984 Kim, S., & Hosseini, S. A. (2014b). Geological CO₂ storage: Incorporation of pore-
985 pressure/stress coupling and thermal effects to determine maximum sustainable pressure
986 limit. *Energy Procedia*, 63, 3339-3346.

987 Kim, S., & Hosseini, S. A. (2015). Hydro-thermo-mechanical analysis during injection of cold
988 fluid into a geologic formation. *International Journal of Rock Mechanics and Mining*
989 *Sciences*, 77, 220-236.

990 Koschel, D., Coxam, J. Y., Rodier, L., & Majer, V. (2006). Enthalpy and solubility data of CO₂
991 in water and NaCl (aq) at conditions of interest for geological sequestration. *Fluid Phase*
992 *Equilibria*, 247(1), 107-120.

993 Krogh, E., Nilsen, R., & Henningsen, R. (2012). Liquefied CO₂ Injection Modelling. *Energy*
994 *Procedia*, 23, 527-555.

995 LaForce, T., Ennis-King, J., & Paterson, L. (2015). Semi-analytical temperature and stress
996 profiles for nonisothermal CO₂ injection. In *Proceedings of the World Geothermal*
997 *Congress*, Melbourne, Australia, 19-25 April 2015.

998 Le Quéré, C., Moriarty, R., Andrew, R. M., et al. (2015). Global carbon budget 2015. *Earth*
999 *System Science Data*, 7(2), 349-396.

1000 Liebscher, A., Möller, F., Bannach, A., Köhler, S., Wiebach, J., Schmidt-Hattenberger, C.,
1001 Weiner, M., Pretschner, C., Ebert, K., & Zemke, J. (2013). Injection operation and
1002 operational pressure–temperature monitoring at the CO₂ storage pilot site Ketzin, Germany
1003 —Design, results, recommendations. *International Journal of Greenhouse Gas Control*,
1004 15, 163-173.

1005 Lindeberg, E. (2011). Modelling pressure and temperature profile in a CO₂ injection well.
1006 *Energy Procedia*, 4, 3935-3941.

1007 Lu, J., Partin, J. W., Hovorka, S. D., & Wong, C. (2010). Potential risks to freshwater
1008 resources as a result of leakage from CO₂ geological storage: a batch-reaction experiment.
1009 *Environmental Earth Sciences*, 60(2), 335-348.

1010 Lu, M., & Connell, L. D. (2008). Non-isothermal flow of carbon dioxide in injection wells
1011 during geological storage. *International journal of greenhouse gas control*, 2(2), 248-258.

1012 Lu, M., & Connell, L. D. (2014a). Transient, thermal wellbore flow of multispecies carbon
1013 dioxide mixtures with phase transition during geological storage. *International Journal of*
1014 *Multiphase Flow*, 63, 82-92.

1015 Lu, M., & Connell, L. D. (2014b). The transient behaviour of CO₂ flow with phase transition
1016 in injection wells during geological storage—Application to a case study. *Journal of*
1017 *Petroleum Science and Engineering*, 124, 7-18.

1018 Luo, Z., & Bryant, S. L. (2010). Influence of thermo-elastic stress on CO₂ injection induced
1019 fractures during storage. In *SPE International Conference on CO₂ capture, storage, and*
1020 *utilization*, New Orleans, Louisiana, 10-12 November 2010.

1021 Luo, Z., & Bryant, S. (2011). Influence of thermo-elastic stress on fracture initiation during
1022 CO₂ injection and storage. *Energy Procedia*, 4, 3714-3721.

1023 Luo, Z., Bryant, S., & Meckel, T. (2013). Application of improved injection well temperature
1024 model to Cranfield measurements. *Energy Procedia*, 37, 4128-4135.

1025 Luo, Z., & Bryant, S. (2013). Can we Overcome Thermo-elastic Limits on CO₂ Injection
1026 Rates in Horizontal Wells?. *Energy Procedia*, 37, 3299-3306.

1027 Luo, Z., & Bryant, S. (2014). Impacts of injection induced fractures propagation in CO₂
1028 geological sequestration—is fracturing good or bad for CO₂ sequestration. *Energy Procedia*,
1029 63, 5394-5407.

1030 Mathias, S. A., Gluyas, J. G., Oldenburg, C. M., & Tsang, C. F. (2010). Analytical solution for
1031 Joule–Thomson cooling during CO₂ geo-sequestration in depleted oil and gas reservoirs.
1032 *International Journal of Greenhouse Gas Control*, 4(5), 806-810.

1033 Mathias, S. A., Gluyas, J. G., González Martínez de Miguel, G. J., & Hosseini, S. A. (2011).
1034 Role of partial miscibility on pressure buildup due to constant rate injection of CO₂ into
1035 closed and open brine aquifers. *Water Resources Research*, 47(12), W12525.

1036 Matter, J. M., Stute, M., Snæbjörnsdóttir, S. Ó., Oelkers, E. H., Gislason, S. R., Aradóttir, E.
1037 S., ... & Axelsson, G. (2016). Rapid carbon mineralization for permanent disposal of
1038 anthropogenic carbon dioxide emissions. *Science*, 352(6291), 1312-1314.

1039 McCoy, S. T., & Rubin, E. S. (2008). An engineering-economic model of pipeline transport of
1040 CO₂ with application to carbon capture and storage. *International Journal of Greenhouse*
1041 *Gas Control*, 2(2), 219-229.

1042 McCulloch, J., Gastineau, J., Bour, D. L., & Ravi, K. (2003). Life cycle modeling of wellbore
1043 cement used for enhanced geothermal system development. *Geothermal Resources*
1044 *Council Transactions*, 27, 147-154.

1045 McPherson, B. J., Han, W. S., & Cole, B. S. (2008). Two equations of state assembled for
1046 basic analysis of multiphase CO₂ flow and in deep sedimentary basin conditions.
1047 *Computers & Geosciences*, 34(5), 427-444.

1048 Miocic, J. M., Gilfillan, S., McDermott, C., & Haszeldine, R. S. (2013). Mechanisms for CO₂
1049 Leakage Prevention—A Global Dataset of Natural Analogues. *Energy Procedia*, 40, 320-
1050 328.

1051 Möller, F., Liebscher, A., Martens, S., Schmidt-Hattenberger, C., & Streibel, M. (2014).
1052 Injection of CO₂ at ambient temperature conditions—pressure and temperature results of the
1053 “cold injection” experiment at the Ketzin pilot site. *Energy Procedia*, 63, 6289-6297.

1054 Munkejord, S. T., Jakobsen, J. P., Austegard, A., & Mølnvik, M. J. (2010). Thermo-and fluid-
1055 dynamical modelling of two-phase multi-component carbon dioxide mixtures.
1056 *International Journal of Greenhouse Gas Control*, 4(4), 589-596.

1057 Nimtz, M., Klatt, M., Wiese, B., Kühn, M., & Joachim Krautz, H. (2010). Modelling of the
1058 CO₂ process-and transport chain in CCS systems—Examination of transport and storage
1059 processes. *Chemie der Erde-Geochemistry*, 70, 185-192.

1060 Nooner, S. L., Eiken, O., Hermanrud, C., Sasagawa, G. S., Stenvold, T., & Zumberge, M. A.
1061 (2007). Constraints on the in situ density of CO₂ within the Utsira formation from time-
1062 lapse seafloor gravity measurements. *International Journal of Greenhouse Gas Control*,
1063 1(2), 198-214.

1064 Nordbotten, J. M., Celia, M. A., & Bachu, S. (2004). Analytical solutions for leakage rates
1065 through abandoned wells. *Water Resources Research*, 40(4).

1066 Nordbotten, J. M., Celia, M. A., Bachu, S., & Dahle, H. K. (2005). Semianalytical solution for
1067 CO₂ leakage through an abandoned well. *Environmental science & technology*, 39(2), 602-
1068 611.

1069 Nuñez-Lopez, V., Muñoz-Torres, J., & Zeidouni, M. (2014). Temperature monitoring using
1070 Distributed Temperature Sensing (DTS) technology. *Energy Procedia*, 63, 3984-3991.

1071 Ochsner, K. (2008). Carbon dioxide heat pipe in conjunction with a ground source heat pump
1072 (GSHP). *Applied Thermal Engineering*, 28(16), 2077-2082.

1073 Oldenburg, C. M. (2007). Joule-Thomson cooling due to CO₂ injection into natural gas
1074 reservoirs. *Energy Conversion and Management*, 48(6), 1808-1815.

1075 Oldenburg, C. M., Doughty, C., Peters, C. A., & Dobson, P. F. (2012). Simulations of long-
1076 column flow experiments related to geologic carbon sequestration: effects of outer wall
1077 boundary condition on upward flow and formation of liquid CO₂. *Greenhouse Gases:
1078 Science and Technology*, 2(4), 279-303.

1079 Osselin, F., Fen-Chong, T., Fabbri, A., Lassin, A., Pereira, J. M., & Dangla, P. (2013).
1080 Dependence on injection temperature and on aquifer's petrophysical properties of the local
1081 stress applying on the pore wall of a crystallized pore in the context of CO₂ storage in deep
1082 saline aquifers. *The European Physical Journal Applied Physics*, 64(02), 21101.

1083 Pan, L., Oldenburg, C. M., Wu, Y. S., & Pruess, K. (2009). Wellbore flow model for carbon
1084 dioxide and brine. *Energy Procedia*, 1(1), 71-78.

1085 Pan, L., Oldenburg, C. M., Pruess, K., & Wu, Y. S. (2011). Transient CO₂ leakage and
1086 injection in wellbore-reservoir systems for geologic carbon sequestration. *Greenhouse
1087 Gases: Science and Technology*, 1(4), 335-350.

1088 Pan, L., & Oldenburg, C. M. (2014). T2Well—an integrated wellbore–reservoir simulator.
1089 *Computers & Geosciences*, 65, 46-55.

1090 Pan, L., Freifeld, B., Doughty, C., Zakem, S., Sheu, M., Cutright, B., & Terrall, T. (2015).
1091 Fully coupled wellbore-reservoir modeling of geothermal heat extraction using CO₂ as the
1092 working fluid. *Geothermics*, 53, 100-113.

1093 Paterson, L., Lu, M., Connell, L., & Ennis-King, J. P. (2008). Numerical modeling of pressure
1094 and temperature profiles including phase transitions in carbon dioxide wells. In *SPE*
1095 *Annual Technical Conference and Exhibition*. Society of Petroleum Engineers.

1096 Paterson, L., Ennis-King, J. P., & Sharma, S. (2010). Observations of thermal and pressure
1097 transients in carbon dioxide wells. In *SPE Annual Technical Conference and Exhibition*.
1098 Society of Petroleum Engineers.

1099 Pekot, L. J., Petit, P., Adushita, Y., Saunier, S., & De Silva, R. L. (2011). Simulation of two-
1100 phase flow in carbon dioxide injection wells. *Offshore Europe*, SPE-144847-MS, 6-8
1101 September, Aberdeen, UK.

1102 Pool, M., Carrera, J., Vilarrasa, V., Silva, O., & Ayora, C. (2013). Dynamics and design of
1103 systems for geological storage of dissolved CO₂. *Advances in Water Resources*, 62, 533-
1104 542.

1105 Preisig, M., & Prévost, J. H. (2011). Coupled multi-phase thermo-poromechanical effects.
1106 Case study: CO₂ injection at In Salah, Algeria. *International Journal of Greenhouse Gas*
1107 *Control*, 5(4), 1055-1064.

1108 Pruess, K., & Garcia, J. (2002). Multiphase flow dynamics during CO₂ disposal into saline
1109 aquifers. *Environmental Geology*, 42(2-3), 282-295.

1110 Pruess, K. (2005a). Numerical studies of fluid leakage from a geologic disposal reservoir for
1111 CO₂ show self-limiting feedback between fluid flow and heat transfer. *Geophysical*
1112 *research letters*, 32(14).

1113 Pruess, K. (2005b). Numerical simulations show potential for strong nonisothermal effects
1114 during fluid leakage from a geologic disposal reservoir for CO₂. *Dynamics of Fluids and*
1115 *Transport in Fractured Rock*, 81-89.

1116 Pruess, K. (2008). On CO₂ fluid flow and heat transfer behavior in the subsurface, following
1117 leakage from a geologic storage reservoir. *Environmental Geology*, 54(8), 1677-1686.

1118 Pruess, K. (2011). Integrated modeling of CO₂ storage and leakage scenarios including
1119 transitions between super- and subcritical conditions, and phase change between liquid and
1120 gaseous CO₂. *Greenhouse Gases: Science and Technology*, 1(3), 237-247.

1121 Randolph, J. B., & Saar, M. O. (2011a). Combining geothermal energy capture with geologic
1122 carbon dioxide sequestration. *Geophysical Research Letters*, 38(10).

1123 Randolph, J. B., & Saar, M. O. (2011b). Coupling carbon dioxide sequestration with
1124 geothermal energy capture in naturally permeable, porous geologic formations:
1125 Implications for CO₂ sequestration. *Energy Procedia*, 4, 2206-2213.

1126 Randolph, J. B., Saar, M. O., & Bielicki, J. (2013). Geothermal energy production at geologic
1127 CO₂ sequestration sites: impact of thermal drawdown on reservoir pressure. *Energy*
1128 *Procedia*, 37, 6625-6635.

1129 Rayward-Smith, W. J., & Woods, A. W. (2011). Some implications of cold CO₂ injection into
1130 deep saline aquifers. *Geophysical Research Letters*, 38(6).

1131 Redlich, O., & Kwong, J. N. (1949). On the thermodynamics of solutions. V. An equation of
1132 state. Fugacities of gaseous solutions. *Chemical reviews*, 44(1), 233-244.

1133 Reinsch, T., Henniges, J., & Ásmundsson, R. (2013). Thermal, mechanical and chemical
1134 influences on the performance of optical fibres for distributed temperature sensing in a hot
1135 geothermal well. *Environmental Earth Sciences*, 70(8), 3465-3480.

1136 Réveillère, A., & Rohmer, J. (2011). Managing the risk of CO₂ leakage from deep saline
1137 aquifer reservoirs through the creation of a hydraulic barrier. *Energy Procedia*, 4, 3187-
1138 3194.

1139 Réveillère, A., Rohmer, J., & Manceau, J. C. (2012). Hydraulic barrier design and
1140 applicability for managing the risk of CO₂ leakage from deep saline aquifers. *International*
1141 *Journal of Greenhouse Gas Control*, 9, 62-71.

1142 Roy, P., Walsh, S. D., Morris, J. P., Iyer, J., Hao, Y., Carroll, S., Gawell, K., Todorovic, J., &
1143 Torsæter, M. (2016). Studying the Impact of Thermal Cycling on Wellbore Integrity during
1144 CO₂ Injection. *Proceedings of the American Rock Mechanics Association*, paper 16-0668,
1145 Houston, Texas, 26-29 June, 2016.

1146 Rutqvist, J., & Tsang, C. F. (2002). A study of caprock hydromechanical changes associated
1147 with CO₂-injection into a brine formation. *Environmental Geology*, 42(2-3), 296-305.

1148 Rutqvist, J., Liu, H. H., Vasco, D. W., Pan, L., Kappler, K., & Majer, E. (2011). Coupled non-
1149 isothermal, multiphase fluid flow, and geomechanical modeling of ground surface
1150 deformations and potential for induced micro-seismicity at the In Salah CO₂ storage
1151 operation. *Energy Procedia*, 4, 3542-3549.

1152 Rutqvist, J. (2012). The geomechanics of CO₂ storage in deep sedimentary formations.
1153 *Geotechnical and Geological Engineering*, 30(3), 525-551.

1154 Saaltink, M. W., Vilarrasa, V., De Gaspari, F., Silva, O., Carrera, J., & Rötting, T. S. (2013). A
1155 method for incorporating equilibrium chemical reactions into multiphase flow models for
1156 CO₂ storage. *Advances in Water Resources*, 62, 431-441.

1157 Sagu, O. L., & Pao, W. K. (2013). In-situ stress perturbation due to temperature around
1158 borehole during carbon injection. *Asian Journal of Applied Sciences*, 6(1), 40-49.

1159 Sasaki, K., Yasunami, T., & Sugaia, Y. (2009). Prediction model of bottom hole temperature
1160 and pressure at deep injector for CO₂ sequestration to recover injection rate. *Energy*
1161 *Procedia*, 1(1), 2999-3006.

1162 Sato, K., Mito, S., Horie, T., Ohkuma, H., Saito, H., Watanabe, J., & Yoshimura, T. (2009). A
1163 monitoring framework for assessing underground migration and containment of carbon
1164 dioxide sequestered in an onshore aquifer. *Energy Procedia*, 1(1), 2261-2268.

1165 Shi, X., & Che, D. (2009). A combined power cycle utilizing low-temperature waste heat and
1166 LNG cold energy. *Energy conversion and management*, 50(3), 567-575.

1167 Silva, O., Carrera, J., & Vilarrasa, V. (2011). An efficient injection concept for the geological
1168 storage of CO₂. *6th Trondheim CCS Conference*, Trondheim, Norway, 14-16 June 2011.

1169 Singh, A. K., Goerke, U. J., & Kolditz, O. (2011a). Numerical simulation of non-isothermal
1170 compositional gas flow: application to carbon dioxide injection into gas reservoirs. *Energy*,
1171 36(5), 3446-3458.

1172 Singh, A. K., Böttcher, N., Wang, W., Park, C. H., Görke, U. J., & Kolditz, O. (2011b). Non-
1173 isothermal effects on two-phase flow in porous medium: CO₂ disposal into a saline aquifer.
1174 *Energy Procedia*, 4, 3889-3895.

1175 Singh, A. K., Baumann, G., Hennings, J., Görke, U. J., & Kolditz, O. (2012). Numerical
1176 analysis of thermal effects during carbon dioxide injection with enhanced gas recovery: a
1177 theoretical case study for the Altmark gas field. *Environmental Earth Sciences*, 67(2), 497-
1178 509.

1179 Skinner, L. (2003). CO₂ blowouts: An emerging problem. *World Oil*, 224(1), 38-42.

1180 Skovholt, O. (1993). CO₂ transportation system. *Energy Conversion and Management*, 34(9),
1181 1095-1103.

1182 Song, J., & Zhang, D. (2012). Comprehensive review of caprock-sealing mechanisms for
1183 geologic carbon sequestration. *Environmental science & technology*, 47(1), 9-22.

1184 Span, R., & Wagner, W. (1996). A new equation of state for carbon dioxide covering the fluid
1185 region from the triple-point temperature to 1100 K at pressures up to 800 MPa. *Journal of*
1186 *physical and chemical reference data*, 25(6), 1509-1596.

1187 Spycher, N., Pruess, K., & Ennis-King, J. (2003). CO₂-H₂O mixtures in the geological
1188 sequestration of CO₂. I. Assessment and calculation of mutual solubilities from 12 to 100°
1189 C and up to 600 bar. *Geochimica et Cosmochimica Acta*, 67(16), 3015-3031.

1190 Spycher, N., & Pruess, K. (2005). CO₂-H₂O mixtures in the geological sequestration of CO₂.
1191 II. Partitioning in chloride brines at 12–100° C and up to 600 bar. *Geochimica et*
1192 *Cosmochimica Acta*, 69(13), 3309-3320.

1193 Svensson, R., Odenberger, M., Johnsson, F., & Strömberg, L. (2004). Transportation systems
1194 for CO₂—application to carbon capture and storage. *Energy Conversion and Management*,
1195 45(15), 2343-2353.

1196 Tao, Q., Bryant, S. L., & Meckel, T. A. (2013). Modeling above-zone measurements of
1197 pressure and temperature for monitoring CCS sites. *International Journal of Greenhouse*
1198 *Gas Control*, 18, 523-530.

1199 Taylor, J., & Bryant, S. (2014). Quantifying thermally driven fracture geometry during CO₂
1200 storage. *Energy Procedia*, 63, 3390-3404.

1201 Teodoriu, C. (2015). Why and When Does Casing Fail in Geothermal Wells: a Surprising
1202 Question?. *Proceedings of World Geothermal Congress 2015*, Melbourne, Australia, 19-25
1203 April 2015.

1204 Tillner, E., Kempka, T., Nakaten, B., & Kühn, M. (2013). Brine migration through fault
1205 zones: 3D numerical simulations for a prospective CO₂ storage site in Northeast Germany.
1206 *International Journal of Greenhouse Gas Control*, 19, 689-703.

1207 Trautz, R. C., Pugh, J. D., Varadharajan, C., Zheng, L., Bianchi, M., Nico, P. S., Spycher, N.
1208 F., Newell, D. L., Esposito, R. A., Wu, Y., Dafflon, B., Hubbard, S. S., & Birkholzer, J. T.

1209 (2012). Effect of dissolved CO₂ on a shallow groundwater system: A controlled release
1210 field experiment. *Environmental Science & Technology*, 47(1), 298-305.

1211 Tutolo, B. M., Kong, X. Z., Seyfried, W. E., & Saar, M. O. (2015). High performance reactive
1212 transport simulations examining the effects of thermal, hydraulic, and chemical (THC)
1213 gradients on fluid injectivity at carbonate CCUS reservoir scales. *International Journal of*
1214 *Greenhouse Gas Control*, 39, 285-301.

1215 Vasco, D. W., Ferretti, A. & Novali, F. (2008). Reservoir monitoring and characterization
1216 using satellite geodetic data: interferometric synthetic aperture radar observations from the
1217 Krechba field, Algeria. *Geophysics*, 73(6), WA113–WA122.

1218 Verdon, J. P., Kendall, J. M., White, D. J., & Angus, D. A. (2011). Linking microseismic event
1219 observations with geomechanical models to minimise the risks of storing CO₂ in geological
1220 formations. *Earth and Planetary Science Letters*, 305(1), 143-152.

1221 Vilarrasa, V., Silva, O., Carrera, J., & Olivella, S. (2013). Liquid CO₂ injection for geological
1222 storage in deep saline aquifers. *International Journal of Greenhouse Gas Control*, 14, 84-
1223 96.

1224 Vilarrasa, V., Olivella, S., Carrera, J., & Rutqvist, J. (2014). Long term impacts of cold CO₂
1225 injection on the caprock integrity. *International Journal of Greenhouse Gas Control*, 24, 1-
1226 13.

1227 Vilarrasa, V., Rutqvist, J., & Rinaldi, A. P. (2015). Thermal and capillary effects on the
1228 caprock mechanical stability at In Salah, Algeria. *Greenhouse Gases: Science and*
1229 *Technology*, 5, 449-461.

1230 Vilarrasa, V., & Carrera, J. (2015). Geologic carbon storage is unlikely to trigger large
1231 earthquakes and reactivate faults through which CO₂ could leak. *Proceedings of the*
1232 *National Academy of Sciences*, 112(19), 5938-5943.

1233 Vilarrasa, V., & Laloui, L. (2015). Potential fracture propagation into the caprock induced by
1234 cold injection in normal faulting stress regimes. *Geomechanics for Energy and the*
1235 *Environment*, 2, 22-31.

1236 Vilarrasa, V., & Laloui, L. (2016). Impacts of thermally induced stresses on fracture stability
1237 during geological storage of CO₂. *Energy Procedia*, 86, 411-419.

1238 Vilarrasa, V. (2016). The role of the stress regime on microseismicity induced by overpressure
1239 and cooling in geologic carbon storage. *Geofluids*, doi: 10.1111/gfl.12197

1240 Wang, H., Shi, X., & Che, D. (2013). Thermodynamic optimization of the operating
1241 parameters for a combined power cycle utilizing low-temperature waste heat and LNG
1242 cold energy. *Applied Thermal Engineering*, 59(1), 490-497.

1243 White, C.M., Smith, D.H., Jones, K.L., Goodman, A.L., Jikich, S.A., LaCount, R.B., DuBose,
1244 S.B., Ozdemir, E., Morsi, B.I., & Schroeder, K.T., (2005). Sequestration of carbon dioxide
1245 in coal with enhanced coalbed methane recovery a review. *Energy & Fuels* 19, 659-724.

1246 White, J.A., Chiamonte, L., Ezzedine, S., Foxall, W., Hao, Y., Ramirez, A., & McNab, W.
1247 (2014). Geomechanical behaviour of the reservoir and caprock system at the In Salah CO₂
1248 storage project. *Proceedings of the National Academy of Sciences*, 111, 8747–8752.

1249 Wiese, B., Nimtz, M., Klatt, M., & Kühn, M. (2010). Sensitivities of injection rates for single
1250 well CO₂ injection into saline aquifers. *Chemie der Erde-Geochemistry*, 70, 165-172.

1251 Wu, Y., & Bryant, S. L. (2014). Optimization of field-scale surface dissolution with
1252 thermoelastic constraints. *Energy Procedia*, 63, 4850-4860.

1253 You, H., Seo, Y., Huh, C., & Chang, D. (2014). Performance analysis of cold energy recovery
1254 from CO₂ injection in ship-based Carbon Capture and Storage (CCS). *Energies*, 7(11),
1255 7266-7281.

1256 Zeidouni, M., Nicot, J. P., & Hovorka, S. D. (2014). Monitoring above-zone temperature
1257 variations associated with CO₂ and brine leakage from a storage aquifer. *Environmental*
1258 *Earth Sciences*, 72:1733–1747.

1259 Zevenhoven, R., Fagerlund, J., & Songok, J. K. (2011). CO₂ mineral sequestration:
1260 developments toward large-scale application. *Greenhouse Gases: Science and Technology*,
1261 1(1), 48-57.

1262 Zhang, W., Li, Y., Xu, T., Cheng, H., Zheng, Y., & Xiong, P. (2009). Long-term variations of
1263 CO₂ trapped in different mechanisms in deep saline formations: a case study of the
1264 Songliao Basin, China. *International journal of greenhouse gas control*, 3(2), 161-180.

1265 Zhang, Z. X., Wang, G. X., Massarotto, P., & Rudolph, V. (2006). Optimization of pipeline
1266 transport for CO₂ sequestration. *Energy Conversion and Management*, 47(6), 702-715.

1267 Zhao, R., & Cheng, J. (2015). Non-isothermal modeling of CO₂ injection into saline aquifers
1268 at a low temperature. *Environmental Earth Sciences*, 73(9), 5307-5316.

1269